Available online at www.sciencedirect.com
ScienceDirect
International Journal of Multiphase Flow 33 (2007) 1365–1394
International Journal of Multiphase Flow
www.elsevier.com/locate/ijmulflow

Parametric study of a model for determining the liquid flow-rates from the pressure drop and water hold-up in oil–water flows

M. Hadžiabdić *, R.V.A. Oliemans

Department of Multi-scale Physics, Delft University of Technology, Prins Bernhardlaan 6, 2628 BW Delft, The Netherlands

Received 25 May 2006; received in revised form 15 July 2007

Abstract

A flow-pattern-dependent model, traditionally used for calculation of pressure drop and water hold-up, is accustomed for calculation of the liquid production rates in oil–water horizontal flow, based on the known pressure drop and water hold-up. The area-averaged steady-state one-dimensional two-fluid model is used for stratified flow, while the homogeneous model is employed for dispersed flow. The prediction errors appear to be larger when the production rates are calculated instead of pressure drop and water hold-up. The difference in the calculation accuracies between the direct and inverse calculation is most probably caused by the different uncertainties in the measured values of the input variables and a high sensitivity of the calculated phase flow-rates on even small change of the water hold-up for certain flow regimes. In order to locate the source of error in the standard two-fluid model formulation, several parametric studies are performed. In the first parametric study, we investigate under which conditions the momentum equations are satisfied when the measured pressure drop and water hold-up are imposed. The second and third parametric studies address the influence of the interfacial waves and drop entrainment on the model accuracy, respectively. These studies show that both interfacial waves and drop entrainment can be responsible for the augmentation of the wall-shear stress in oil–water flow. In addition, consideration of the interfacial waves offers an explanation for some important phenomena of the oil–water flow, such as the wall-shear stress reduction.

Keywords: Two-fluid model; Oil and water production rates; Oil–water horizontal flow

1. Introduction

The optimisation of oil production logging strongly depends on a reliable estimation of the oil and water production rates in tubing at angles from horizontal up to vertical. The presence of water in the down-hole

* Corresponding author. Present address: International University of Sarajevo, Paromlinska 66, 71000 Sarajevo, Bosnia and Herzegovina.
E-mail addresses: M.Hadziabdic@tudelft.nl, mhadziabdic@ius.edu.ba (M. Hadžiabdić).

0301-9322/$ - see front matter © 2007 Elsevier Ltd. All rights reserved.
doi:10.1016/j.ijmultiphaseflow.2007.07.003

producing wells is likely to occur as oil fields have reached their mature phase. The accurate prediction of the oil and water flow-rates appears not to be an easy task since the oil and water production rates depend strongly on factors such as oil and water properties, pipe material, pipe diameter, Reynolds number of each phase, etc. Usually, these factors interact with one another leading to complex relationships.

In contrast to the extensively studied gas–liquid flows, topics regarding liquid–liquid flow received less attention, despite the relevance of the flow, both for industrial applications and for understanding of the fundamental physics of the multi-phase flow. Brauner and Moalem Maron (1991) first proposed the liquid–liquid flow-pattern-transition model. The transition from a stratified flow to other flow configurations is described by parameters obtained from the stability analysis and well posedness of the two-fluid model equations. Comparisons of the model results with available experimental data were satisfactory.

Trallero (1995) introduced the flow-pattern model for oil–water flow based on the Kelvin–Helmholtz stability analysis of the interface for liquid–liquid flow. The model was applied to horizontal and slightly inclined flows with moderate success. It was stressed that the model is not suitable for low or high values of h_w/D (h_w is water-layer height, D is pipe diameter) due to the damping effect of the pipe wall. This makes the sheltering approximation not valid.

Apart from a model for predicting the flow pattern, closure relations are needed for the wall- and interfacial-shear stresses. Single-phase based closure relations are commonly used even though their limitations have long been recognised. The widely used closure relations do not account for the physical phenomena characteristic for the multi-phase flow, such as interfacial waves, entrainment of droplets of opposite phase and curved interface. Deficiencies of the commonly used closure relations were reported by Ullmann et al. (2003) and Ullmann and Brauner (2004) among others. Recently, Ullmann and Brauner (2006) proposed new closure relations for the two-fluid model for stratified-smooth and stratified-wavy flows. The new empirical correlations were introduced to account for the wave effects on the interface curvature, the interfacial-shear and the liquid wall-shear stresses. However, the empirical correlations were derived based on gas–liquid experimental data. Since the liquid–liquid flow significantly differs from the gas–liquid system, some of the model coefficients need to be re-calibrated.

A flow-pattern-dependent model is traditionally used for predicting the flow pattern along with the pressure loss and the phase hold-ups in pipes at different angles. The prediction accuracy depends on the accurate prediction of the oil–water flow pattern. Based on the flow-pattern prediction, the two-fluid model (for the stratified flow) or the homogeneous model (for the dispersed flow) is employed. Recent technological developments aim to determine the down-hole pressure loss and phase hold-ups, which would open a space for model prediction of the oil and water production rates from limited down-hole information. The aim of this work is to develop a method for computing the oil and water superficial velocities based on pressure gradient and hold-up information in horizontal oil–water flows. This practice is denoted as inverse modelling.

Rodriguez et al. (2004) presented the principle of inverse modelling and applied it to available oil–water horizontal pipe flow data (Elseth, 2001; Trallero, 1995). The agreement with experimental data was satisfactory. However, the applied methodology did not always ensure a unique solution. The methodology was also not straightforward since the resulting superficial velocities had to be obtained through a graphical interpretation.

Guet et al. (2006) used a subset of dispersed flow data from the Rodriguez and Oliemans (2006) measurements to assess the capability of applying the inverse technique to determine oil–water flow-rates. A hybrid water-cut-dependent model was introduced for the effective viscosity of a water-in-oil dispersion valid up to the inversion point determined with a literature correlation. The proposed reconstruction method is straightforward since the mixture velocity is obtained directly from the momentum equation. The velocities for all pipe inclinations were reconstructed with an accuracy of 50%, while for the case of horizontal flow an accuracy of 17% was achieved.

The focus of this work is on the stratified and dual continuous oil–water flow in a horizontal pipe. The reconstruction method is developed for the prediction of the oil and water superficial velocities. The prediction accuracies with the base flow-pattern dependent model are investigated alongside with the possibility to improve the two-fluid model by accounting for the interfacial waves and drop entrainment. Several parametric studies are conducted in order to assess the influence of oil–water interface related phenomena, such as the interfacial waves and drop entrainment, on the model accuracy.

2. The flow-pattern-dependent method

The flow-pattern-dependent method uses two sub-models, the homogeneous model for dispersed flows and the two-fluid model for stratified flows. Based on the predicted flow pattern, the appropriate sub-model is employed. The Trallero model for prediction of the flow patterns is used in this work.

2.1. Two-fluid model

In the two-fluid approach, the momentum equations are solved for each phase with an assumption that no mixing occurs at the interface. The interface is assumed to be flat. The momentum equations for the two fluids can be written as

$$-\frac{\mathrm{d}P}{\mathrm{d}x}+\tau_{\mathrm{u}}\frac{S_{\mathrm{u}}}{A_{\mathrm{u}}}\pm\tau_{\mathrm{i}}\frac{S_{\mathrm{i}}}{A_{\mathrm{u}}}+\rho_{\mathrm{u}}g\sin\alpha=0, \tag{1}$$

$$-\frac{\mathrm{d}P}{\mathrm{d}x}+\tau_{\mathrm{l}}\frac{S_{\mathrm{l}}}{A_{\mathrm{l}}}\mp\tau_{\mathrm{i}}\frac{S_{\mathrm{i}}}{A_{\mathrm{l}}}+\rho_{\mathrm{l}}g\sin\alpha=0, \tag{2}$$

where P is the pressure, τ stands for the wall-shear stress, S_{u} and S_{l} are the wall perimeters of the upper and lower fluids respectively, S_{i} is the interfacial perimeter, A is the cross-sectional area, ρ is the density, g is the gravitational acceleration and α is the inclination angle from the horizontal. The subscripts[1] u, l and i refer to the upper phase, the lower phase and the interface, respectively.

Eliminating the pressure drop from Eqs. (1) and (2), the following equation is obtained:

$$-\tau_{\mathrm{l}}\frac{S_{\mathrm{l}}}{A_{\mathrm{l}}}+\tau_{\mathrm{u}}\frac{S_{\mathrm{u}}}{A_{\mathrm{u}}}\pm\tau_{\mathrm{i}}S_{\mathrm{i}}\left(\frac{1}{A_{\mathrm{u}}}+\frac{1}{A_{\mathrm{l}}}\right)-(\rho_{\mathrm{l}}-\rho_{\mathrm{u}})g\sin\alpha=0. \tag{3}$$

The wall-shear stresses acting on each phase are expressed as a function of the phase bulk-velocity U and a corresponding friction factor f:

$$\tau=\frac{1}{2}f\rho U|U|. \tag{4}$$

The friction factor f is calculated by the Haaland (1983) formula:

$$f=\begin{cases}\frac{16}{Re} & \text{if } Re<1500,\\ \left\{-3.6\log_{10}\left[\frac{6.9}{Re}+\left(\frac{e}{3.7D_{\mathrm{h}}}\right)^{1.1}\right]\right\}^{-2} & \text{if } Re>1500,\end{cases} \tag{5}$$

where D_{h} is the hydraulic diameter, $Re=\frac{\rho D_{\mathrm{h}}U}{\nu}$ is the phase-Reynolds number and e is the pipe-wall roughness. The friction factor f is calculated using definitions of the equivalent hydraulic diameters (Brauner and Moalem Maron, 1991):

$$\text{for } U_{\mathrm{l}}>U_{\mathrm{u}},\quad D_{hl}=\frac{4A_{\mathrm{l}}}{S_{\mathrm{l}}+S_{\mathrm{i}}}\quad\text{and}\quad D_{\mathrm{hu}}=\frac{4A_{\mathrm{u}}}{S_{\mathrm{u}}}, \tag{6}$$

$$\text{for } U_{\mathrm{l}}<U_{\mathrm{u}},\quad D_{hl}=\frac{4A_{\mathrm{l}}}{S_{\mathrm{l}}}\quad\text{and}\quad D_{\mathrm{hu}}=\frac{4A_{\mathrm{u}}}{S_{\mathrm{u}}+S_{\mathrm{i}}}. \tag{7}$$

For the interfacial-shear stress, the closure relation is

$$\tau_{\mathrm{i}}=\frac{1}{2}f_{\mathrm{i}}\rho_f(U_{\mathrm{l}}-U_{\mathrm{u}})^2, \tag{8}$$

where f_{i} and ρ_{f} are taken equal to the friction factor and density of the faster moving phase respectively.

[1] For the standard two-fluid model subscripts u and l correspond to oil and water, respectively.

2.2. Homogeneous model

The homogeneous model treats a mixture of the phases as a single fluid with the average properties defined as

$$\rho_m = \varepsilon_o \rho_o + \varepsilon_w \rho_w, \tag{9}$$

$$U_m = U_{os} + U_{ws}, \tag{10}$$

where $\varepsilon_w = \frac{A_w}{A}$ and $\varepsilon_o = \frac{A_o}{A}$ are water and oil hold-ups, $U_{os} = \frac{A_o U_o}{A}$ and $U_{ws} = \frac{A_w U_w}{A}$ are water and oil superficial velocities respectively.

The pressure drop is calculated as

$$\frac{dP}{dx} = -\frac{2 f_m \rho_m U_m^2}{D} - \rho_m g \sin\alpha, \tag{11}$$

where f_m is calculated by Eq. (5) based on the mixture Reynolds number $Re_m = \frac{\rho_m D U_m}{\nu_m}$.

The transition from water-in-oil to oil-in-water dispersion is determined by the correlation for the critical water cut proposed by Arirachakaran et al. (1989):

$$C_{w,crit} = 0.5 - 0.1108 \log_{10}\left(\frac{\mu_o}{\mu_w}\right). \tag{12}$$

If the water cut $C_w = (\frac{U_{ws}}{U_{ws}+U_{os}})$ is smaller than $C_{w,crit}$, dispersion is denoted as Dw/o, otherwise as Do/w. The hybrid water-cut dependent model, proposed by Guet et al. (2006), is used to calculate the mixture viscosity (μ_m) needed to determine the mixture-Reynolds number. The mixture viscosity for a dispersion of water in oil is defined as

$$\mu_m = \begin{cases} (1 + 2.5\varepsilon_d + 14.1\varepsilon_d^2)\mu_c & \text{if } \varepsilon_d < \varepsilon_{d,c}, \\ [(1 + 2.5\varepsilon_{d,c} + 14.1\varepsilon_{d,c}^2)\mu_c](1 - \Phi) + [\mu_d \varepsilon_{d,e} + \mu_d(1 - \varepsilon_{d,e})]\Phi & \text{if } \varepsilon_d > \varepsilon_{d,c} \end{cases} \tag{13}$$

in which ε_d is the hold-up of the dispersed phase, $\varepsilon_{d,c}$ is the maximum dispersed phase volume fraction for which drop break-up due to turbulence dominates over drop coalescence, $\varepsilon_{d,e}$ is a fraction of large drops and Φ is an indication of the relative fraction of large drops present in the mixture. Guet et al. (2006), based on previous work of Brauner (2001), estimated $\varepsilon_{d,c} \approx 0.089$. $\varepsilon_{d,e}$ is estimated as

$$\varepsilon_{d,e} = \varepsilon_d - \varepsilon_{d,c}, \tag{14}$$

while Φ is estimated by

$$\Phi = \frac{\varepsilon_d - \varepsilon_{d,c}}{\varepsilon_d}. \tag{15}$$

2.3. Reconstruction technique for the oil and water flow-rates

The prediction of pressure drop and water hold-up, by the flow-pattern-dependent model, is straightforward since the oil and water velocities, needed for the flow-pattern prediction, are known variables. Fig. 1a schematically shows the algorithm for the pressure drop and water hold-up calculations.

If the oil and water velocities need to be estimated based on the known pressure drop and water hold-up, the flow pattern cannot be estimated directly but an iterative procedure has to be developed. The algorithm for calculation of the oil and water flow-rates is presented schematically in Fig. 1b. The velocities obtained by the two-fluid model proved to be more reliable for the determination of the flow pattern than the velocities calculated by the homogeneous model. The flow-pattern dependent model applies the homogeneous model if the flow is predicted to be fully dispersed.

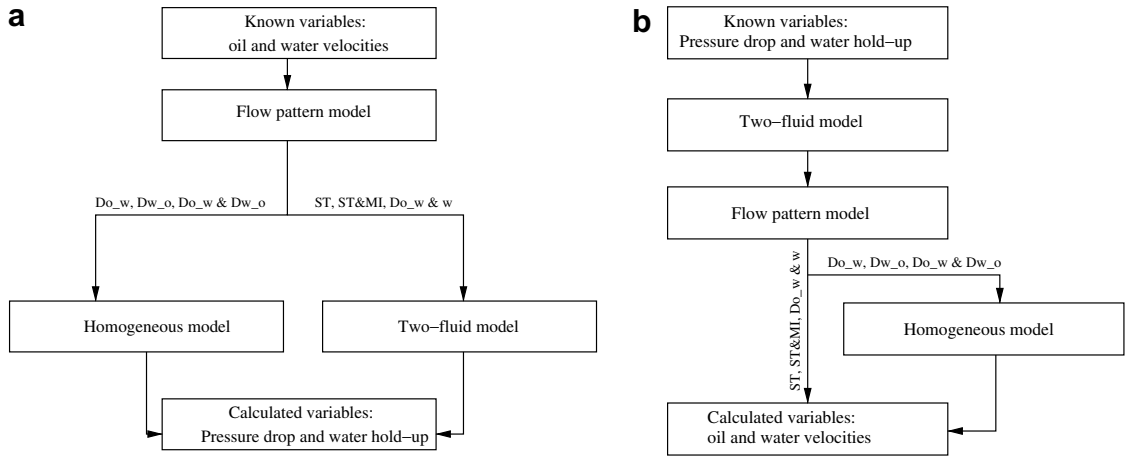

Fig. 1. (a) Schematic description of the algorithm for calculation of pressure drops and water hold-ups; (b) schematic description of the algorithm for calculation of oil and water flow-rates.

3. The results of the flow-pattern-dependent model

3.1. Calculation of pressure drop and water hold-up

A set of experimental data collected by Rodriguez and Oliemans (2006) for horizontal and slightly inclined oil–water pipe flow of diameter $D_p = 0.0828$ m and length $L = 15.5$ m is used for model validation. The data were collected in the Donau multi-phase flow loop (Shell Rijswijk, The Netherlands). The oil and water properties used in the experiment were $\mu_o = 7.5$ mPa s, $\rho_o = 830$ kg/m^3, $\mu_w = 0.8$ mPa s, $\sigma = 0.02$ N/m and $\rho_w = 1060$ kg/m^3. Steady-state data on flow patterns, two-phase pressure gradient and water hold-up were obtained over a wide range of flow-rates for pipe inclinations of $-5°$, $-2°$, $-1.5°$, $0°$, $1°$, $2°$, $5°$. The characterisation of flow patterns and identification of flow-pattern boundaries were achieved via observation of recorded movies and by analysis of the relative deviation from the homogeneous behavior. The values predicted by the model are compared to the experimental data using the averaged relative error:

$$e = \sum 100 \cdot \frac{\sqrt{\left(\frac{\phi_{mod} - \phi_{exp}}{\phi_{exp}}\right)^2}}{N} [\%], \tag{16}$$

where ϕ is a comparing variable, the subscript mod indicates model prediction, the subscript exp indicates the corresponding experimentally measured value and N is the number of the experimental points used for comparison.

The oil–water flow patterns observed in the experiments were in line with the flow-pattern classification proposed by Trallero (1995):

Stratified smooth	ST
Stratified wavy	SW
Stratified flow with mixing at the interface	ST&MI
Dispersion of oil in water and water	Do/w & w
Dispersion of oil in water	Do/w
Dispersion of water in oil	Dw/o
Dispersion of water in oil and oil in water	Do/w & Dw/o

Fig. 2 presents the results obtained with the flow-pattern-dependent model for horizontal-pipe flow. Prediction of the flow patterns by the Trallero model is shown in Fig. 2a. An error in predicting flow pattern is calculated by

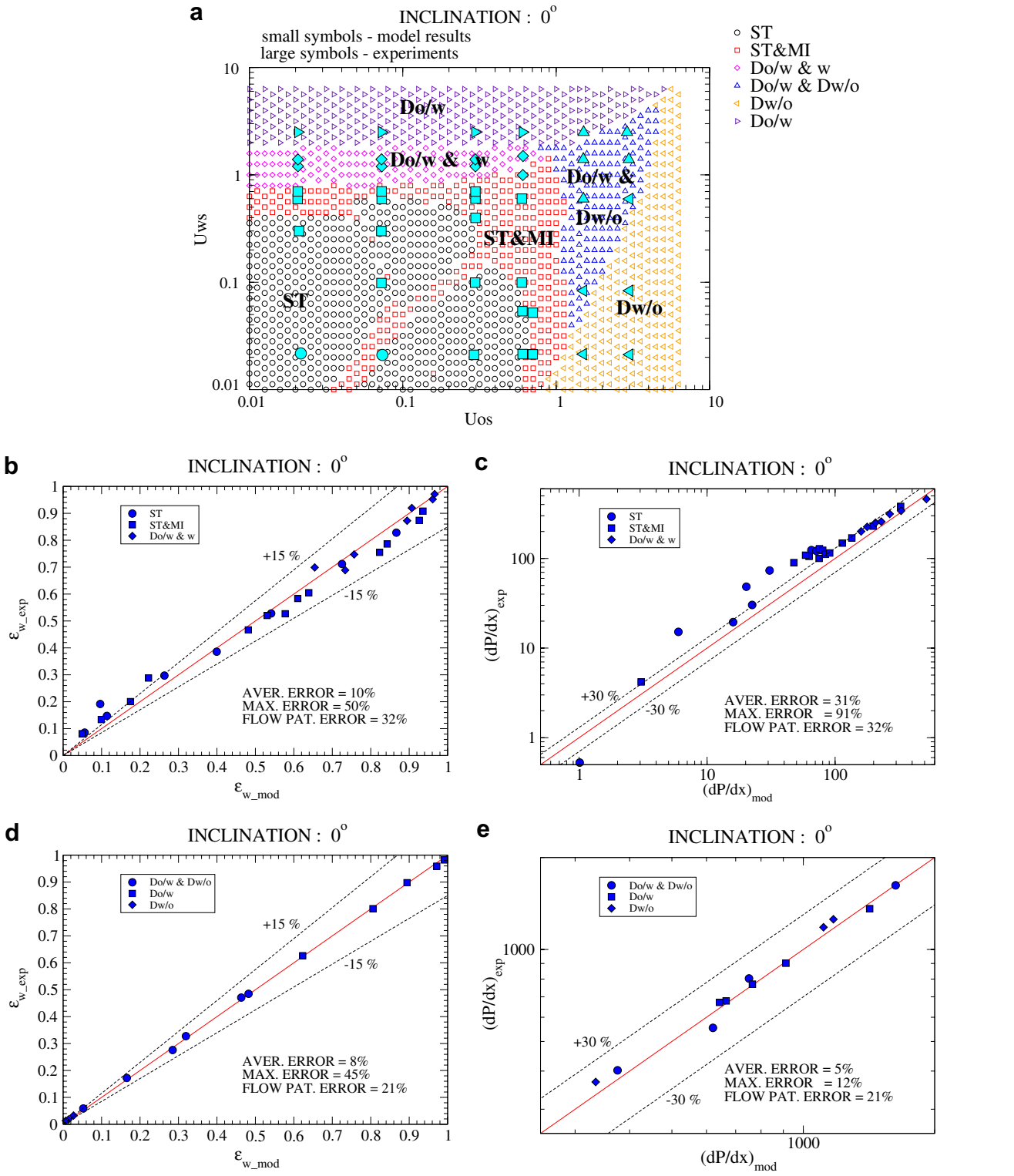

Fig. 2. (a) The flow map predicted by the Trallero model; (b) the water hold-up predicted by the two-fluid model; (c) the pressure drop predicted by the two-fluid model; (d) the water hold-up predicted by the homogeneous model; (e) the pressure drop predicted by the homogeneous model.

$$e_{fp} = \frac{N - N_{\text{corr}}}{N} 100[\%], \tag{17}$$

where N is the number of the experimental points used for comparison and N_{corr} is the number of points for which the flow pattern is correctly predicted. The overall agreement between the experimental flow map and that predicted by the model is 72%. The dispersed flow patterns (Do/w & Dw/o, Do/w and Dw/o) are more accurately predicted (20% error) than the flow patterns in which one or two continuous layers exist such as ST, ST&MI and Do/w & w (obtained accuracy is 68%). It can be noticed that the most pronounced disagreement appears in the prediction of the border between the ST and ST&MI regions. The model significantly overestimates the size of the stratified region in the flow map. This reveals the difficulties to predict accurately the occurrence of drop entrainment at the oil–water interface. The other borders between different flow patterns are relatively well predicted with a small overestimation of the Do/w & Dw/o region. It is interesting to notice penetration of the ST&MI region into the ST region. This was not visible in the Rodriguez and Oliemans (2006) results even though the same model was used as in this research. The reason for this is in the resolution of the calculated velocity pairs ($U_{\text{os}}, U_{\text{ws}}$). We performed the calculation over the same velocity interval but with a much larger number of the velocity pairs ($U_{\text{os}}, U_{\text{ws}}$).

It is not obvious which model, two-fluid or homogeneous, should be applied in case of the Do/w & Dw/o and Do/w & w flow patterns. Both flow patterns belong to dual-continuous flows. These flow patterns do not satisfy conditions under which either the homogeneous or two-fluid model is derived. However, it was found by Rodriguez and Oliemans (2006) that the Do/w & Dw/o behaves as dispersed flow, while the Do/w & w presents an ambiguous behavior in terms of slip and might be treated as either stratified or dispersed flow. It appears that the homogeneous model produces better results for the experimental points in the Do/w & Dw/o region, while the two-fluid model is more suited for predicting the points in the Do/w & w region. Therefore, the Do/w & Dw/o flow pattern is treated as a single phase and the homogeneous model is used to calculate the mixed viscosity and density while for the Do/w & w flow pattern it is assumed that the interface between phases exists and the standard two-fluid model is applied. The results obtained with both models for these flow patterns, are presented in Tables 1 and 2.

Fig. 2b and c show the results for the water hold-up and pressure drop calculations, for the experimental points predicted to be in the ST, ST&MI and Do/w & w regions. For these points, the two-fluid model is used. The prediction of the water hold-up is relatively satisfactory with an averaged error of 10%. However, the maximum deviation is high. It occurs for the experimental points with water hold-ups smaller than 0.1. The pressure drop is predicted with an averaged accuracy of 31%. However, the maximum deviation is also high (91%). The high prediction errors occur for the experimental points with $\frac{dP}{dx} < 100$ Pa/m, while the experimental points with $\frac{dP}{dx} > 100$ Pa/m have errors smaller than 30%. All the points with a pressure gradient smaller than 100 Pa/m belong to the ST and ST&MI regions. For these points, the model underestimates the wall-shear stress (and consequently the pressure gradient) for all the experimental points except one.

The two-fluid model fails to predict accurately the pressure drop and the water hold-up for almost all experimental points with small or high values of the water hold-up. Since the oil–water interface is located in the proximity of the thinner-layer-wetted wall, phenomena such as the interface waves, entrainment or curved interface, may strongly affect the wall- and interfacial-shear stresses. However, the base two-fluid model does not account for these phenomena. The underprediction of the wall-shear stress allows fluid to flow faster, which leads to underprediction of the hold-up of the corresponding phase.

Table 1
Results for the experimental points with Do/w & Dw/o flow patter

–		Two-fluid model	Homogeneous model
$\frac{dP}{dx}$	Averaged error [%]	14.4	8.4
	Maximal error [%]	27.2	15.5
ε_{w}	Averaged error [%]	4.4	1.6
	Maximal error [%]	9.8	3.2
U_{os}	Averaged error [%]	11.5	4.0
	Maximal error [%]	23.0	7.4
U_{ws}	Averaged error [%]	8.4	4.8
	Maximal error [%]	13.8	10.6

Table 2
Results for the experimental points with Do/w & w flow patter

–		Two-fluid model	Homogeneous model
$\frac{dP}{dx}$	Averaged error [%]	14.0	16.7
	Maximal error [%]	20.0	32.5
ε_w	Averaged error [%]	3.6	7.8
	Maximal error [%]	9.7	18
U_{os}	Averaged error [%]	26	94
	Maximal error [%]	54	212
U_{ws}	Averaged error [%]	5.4	4
	Maximal error [%]	11	6.8

Fig. 2d and e show the predicted water hold-up and pressure drop for the experimental points belonging to the dispersed flow regimes. The maximum deviation in the water hold-up predictions is 45% and it occurs for points with water hold-up smaller than 0.1. However, the averaged error is relatively small, which means that high model errors occur only for few experimental points. The predictions for the pressure drop are also more accurate than for the experimental points in the ST, ST&MI and Do/w & w regions. The maximum deviation is 12% while the averaged error is 5%.

Dispersed flow occurs when the turbulent kinetic energy is sufficiently large to mix the phases and produce a dispersion. The turbulent mixing reduces the slip between phases, which diminishes the effect of the interfacial-shear stress on the momentum balance. In the dispersed flow, the wall-shear stress is mainly determined by turbulence. The dominance of the Reynolds (turbulent) shear stress over the other components of the total shear stress (such as the viscous component and components due to the periodic flow when interfacial waves exist) and the fact that the interfacial-shear stress can be neglected due to the small phase-velocity difference, makes the dispersed flow somewhat easier to model. This is the main reason for more successful model predictions of the pressure drop and water hold-up for the experimental points in the dispersed flow regimes.

3.2. Calculation of oil and water flow-rates

If the oil and water velocities need to be calculated by the flow-patter-dependent model, an iterative procedure, described in Fig. 1b, has to be applied. The same theoretical flow map, shown in Fig. 2a, is presented in Fig. 3a in the $\frac{dP}{dx} - \varepsilon_w$ coordinates. This is a more appropriate representation of the flow map since it is assumed that the pressure gradient and water hold-up are the known variables. The model prediction of the flow patterns is satisfactory, with an error of 24%.

Fig. 3b and c show predictions of the oil and water superficial velocities respectively, for the experimental points predicted by the model to belong to the ST, ST&MI and Do/w & w regions. Average errors for both phase-velocities are about 45% but the maximum deviations are very high. The experimental points in the dispersed flow regions are more accurately predicted with an average error of 15% for both superficial velocities and maximum deviations of 122% and 96% for the oil and water superficial velocities, respectively.

Such poor model accuracy, especially for the points in the ST or ST&MI regions, is surprising, since the maximum deviation when the pressure drop and water hold-up are calculated, is an order of magnitude smaller. The disagreement with the measured velocities is largest for the flow conditions with one or both phase-superficial velocities smaller than 0.3 m/s. Fig. 3a shows that the experimental points with the prediction errors smaller than 30% are located mainly in the region defined by $\frac{dP}{dx} > 100$ Pa/m and $0.2 < \varepsilon_w < 0.8$.

Since the same mathematical model is used, we expected model accuracies to be similar to those obtained when the pressure drop and water hold-up are calculated. In order to understand the reasons for the higher prediction errors when the superficial velocities are calculated, we investigate the sensitivity of the calculated variables to a small change in the values of the input variables. In order to simplify the sensitivity estimation, we focus on the dependence of the calculated water flow-rate on the input values of the water hold-up and vice-versa. The data plotted in Fig. 4 are obtained by the two-fluid-model calculation in which the flow-rate of the oil phase is kept constant while the flow-rate of the water phase is varying (the pressure drop and water hold-up are then calculated). Fig. 4a and b show the values of ε_w depending on the water flow-rate and vice-

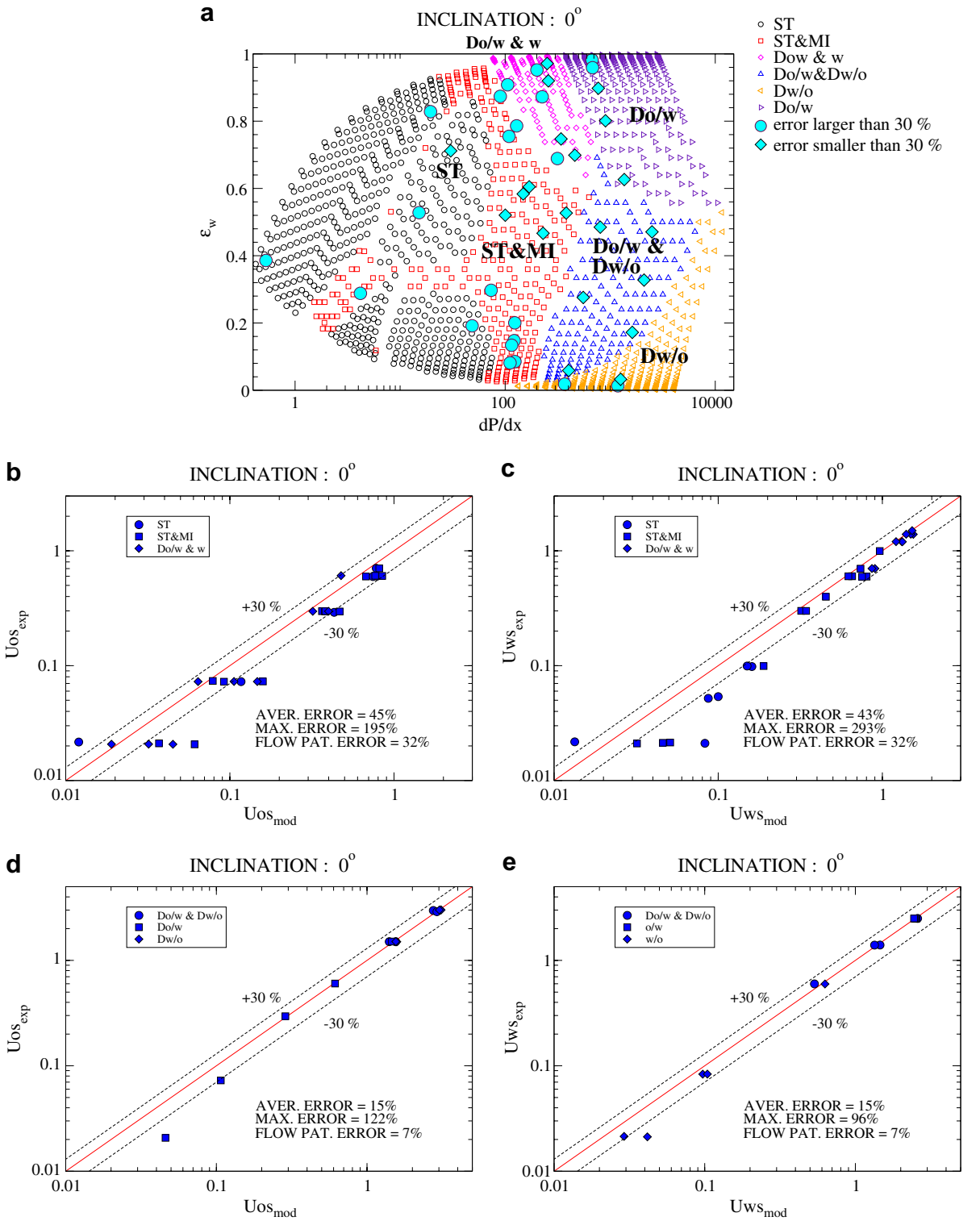

Fig. 3. (a) The flow map predicted by the Trallero model; (b) the oil superficial velocities predicted by the two-fluid model; (c) the water superficial velocities predicted by the two-fluid model; (d) the oil superficial velocities predicted by the homogeneous model; (e) the water superficial velocities predicted by the homogeneous model.

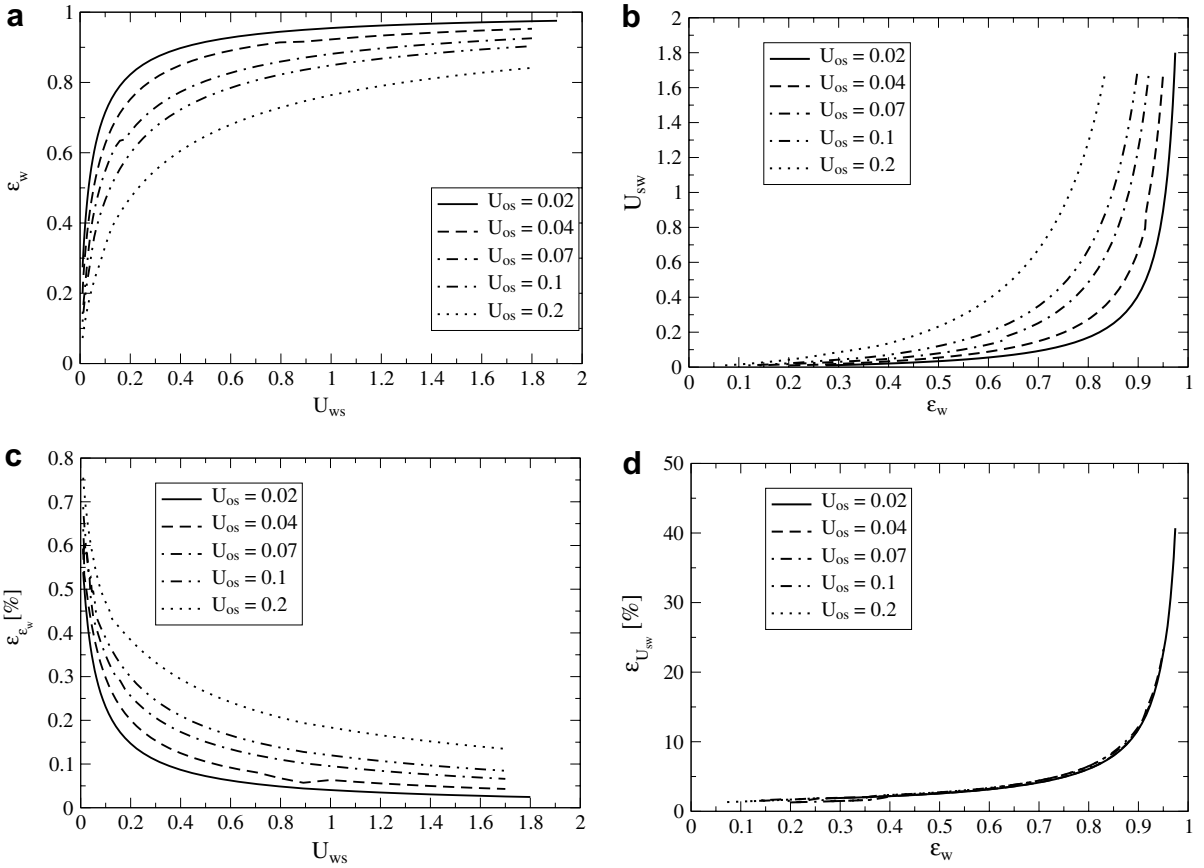

Fig. 4. (a, b) Two-fluid model results for the constant oil flow-rates, (c) estimated uncertainty for the water hold-up normalized by the corresponding value of ε_w, (d) estimated uncertainty for the water flow-rate normalized by the corresponding value of U_{ws}.

versa. We use the Taylor's theorem for estimation of the calculated water hold-up/flow-rate sensitivity to the small change in the input values of the water flow-rate/hold-up.

According to Taylor's theorem, a general function f can be expressed as follows:

$$f[(x_1+\varepsilon_1),(x_2+\varepsilon_2),\cdots,(x_n+\varepsilon_n)] = f(x_1,x_2,\cdots,x_n) + \varepsilon_1\frac{\partial f}{\partial x_1} + \varepsilon_2\frac{\partial f}{\partial x_2} + \cdots + \varepsilon_n\frac{\partial f}{\partial x_n} + \frac{\varepsilon_1^2}{2}\frac{\partial^2 f}{\partial x_1^2} + \frac{\varepsilon_2^2}{2}\frac{\partial^2 f}{\partial x_2^2} + \ldots + \frac{\varepsilon_n^2}{2}\frac{\partial^2 f}{\partial x_n^2} + \cdots, \tag{18}$$

where x_n stands for n variables, and ε_n is the uncertainty in each of these variables. If the higher order terms are neglected and it is assumed that the probability of positive and negative uncertainty is equal, the overall uncertainty can be defined as

$$\varepsilon_f = f[(|x_1|+|\varepsilon_1|),(|x_2|+|\varepsilon_2|),\ldots,(|x_n|+|\varepsilon_n|)] - f(|x_1|,|x_2|,\ldots,|x_n|) = \varepsilon_1\frac{\partial f}{\partial x_1} + \varepsilon_2\frac{\partial f}{\partial x_2} + \cdots + \varepsilon_n\frac{\partial f}{\partial x_n}. \tag{19}$$

Using Eq. (19), the calculation sensitivity for ε_w and U_{ws} can be estimated as follows:

$$\varepsilon_{\varepsilon_w} = \frac{\partial \varepsilon_w}{\partial U_{ws}}\varepsilon_{U_{ws}} + \frac{\partial \varepsilon_w}{\partial U_{os}}\varepsilon_{U_{os}}, \tag{20}$$

$$\varepsilon_{U_{ws}} = \frac{\partial U_{ws}}{\partial \varepsilon_w}\varepsilon_{\varepsilon_w} + \frac{\partial U_{ws}}{\partial (dp/dx)}\varepsilon_{(dp/dx)}, \tag{21}$$

where $\varepsilon_{U_{ws}}$, $\varepsilon_{U_{os}}$, $\varepsilon_{(dp/dx)}$ and $\varepsilon_{\varepsilon_w}$ are the uncertainties in the water flow-rate, oil flow-rate, pressure drop and water hold-up respectively. The second term in Eq. (20), which represents the calculation uncertainty due the uncertainty in the input oil flow-rate, is neglected since we assume that there is nouncertainty in the input oil flow-rates. The second term in Eq. (21) is also assumed to be zero in order to more clearly see the consequences of the inverse calculation on ε_w and U_{ws}. Both uncertainties, $\varepsilon_{U_{ws}}$ and $\varepsilon_{\varepsilon_w}$, are taken to be equal to 1% of the measured values:

$$\varepsilon_{U_{ws}} = 0.01 U_{ws}, \tag{22}$$

$$\varepsilon_{\varepsilon_w} = 0.01 \varepsilon_w. \tag{23}$$

The gradients $\frac{\partial \varepsilon_w}{\partial U_{ws}}$ and $\frac{\partial U_{ws}}{\partial \varepsilon_w}$ can be calculated from the data plotted in Fig. 4a and b.

Fig. 4c and d show the estimated uncertainties by Eqs. (20) and (21), normalized by the corresponding values of the water flow-rates and water hold-up. It can be seen that the influence of the small change in the water flow-rate on the calculated water hold-up is small. The estimated uncertainty for the water hold-up is smaller than 1% for all considered values of water and oil flow-rates, see Fig. 4c. However, Fig. 4d reveals that even 1% change in the values of ε_w can cause the calculation uncertainty as high as 40%. It is interesting to notice that the estimated uncertainty for the water flow-rate is the same for different values of the oil flow-rates. It increases with the increase of the water hold-up. Knowing that the highest uncertainty in measuring ε_w (around 8%) is present for small and high values of the water hold-up (Rodriguez and Oliemans, 2006), it can be expected that the measuring error can significantly influence the calculation error when the phase flow-rates are calculated by the two-fluid model. We assume that the difference in the calculation accuracies between the direct and inverse calculation is caused by the different uncertainties in the measured values of the input variables and a high sensitivity of the calculated phase flow-rates on even small change of the water hold-up for certain flow regimes. This assumption is supported by the fact that an accuracy of the inverted method is approximately the same as the accuracy of the standard method for a sufficiently high pressure drop and moderate values of the water hold-up, see Fig. 3a.

4. A parametric study of the two-fluid model

A parametric study is made for the experimental points which flow pattern is denoted as stratified, in order to determine the values of the oil and water wall-shear stresses that satisfy the two-fluid model equations when the measured pressure drop and water hold-up are imposed. The same model equations, described in Section 2.1, are used except that the oil and water wall-shear stresses are defined as

$$\tau_w = \tau_{w,sp} + \Delta\tau_w, \tag{24}$$

$$\tau_o = \tau_{o,sp} + \Delta\tau_o, \tag{25}$$

where $\tau_{w,sp}$ and $\tau_{o,sp}$ are the wall-shear stresses calculated by Eq. (4), $\Delta\tau_w$ and $\Delta\tau_o$ are parameters that can be both positive or negative and τ_w and τ_o are the total wall-shear stresses on the water and oil sides, respectively. The subscript sp stands for single-phase. The closure relation (4) was derived for single-phase, wall-attached, equilibrium flows such as the flows in pipes or channels. The wall-shear-stress component τ_{sp} is a wall-shear stress that would be caused by the single-phase flow with the same Reynolds number and hydraulic diameter as the corresponding phase has. The closure relation (4) is well founded for the multi-phase flow as long as the flow dynamics and resulted flow structures are similar to those that exist in the single-phase flow. However, the existence of the oil–water interface and related phenomena, such as the interfacial-shear stress, entrainment and interfacial waves, makes the flow of oil and water in the upper and lower layers significantly different from an equivalent (with the same Reynolds number and hydraulic diameter) single-phase flow. The wall-shear-stress component $\Delta\tau$ represents the part of the wall-shear stress that is related to the multi-phase flow phenomena and cannot be anticipated by the closure relation (4).

The parameters $\Delta\tau_w$ and $\Delta\tau_o$ are calculated directly based on the specified (experimental) flow-rates and data of pressure gradient and hold-up via two-fluid model equations. The resulting oil and water wall-shear-stress components ($\tau_{sp}, \Delta\tau$), normalized by the total shear stresses ($\tau_{sp} + \Delta\tau$), are presented in Fig. 5. The component $\Delta\tau$ is non-zero for almost all experimental points. The contribution of each component to the total wall-shear stress can be seen in Fig. 5. It is important to notice that for some experimental points,

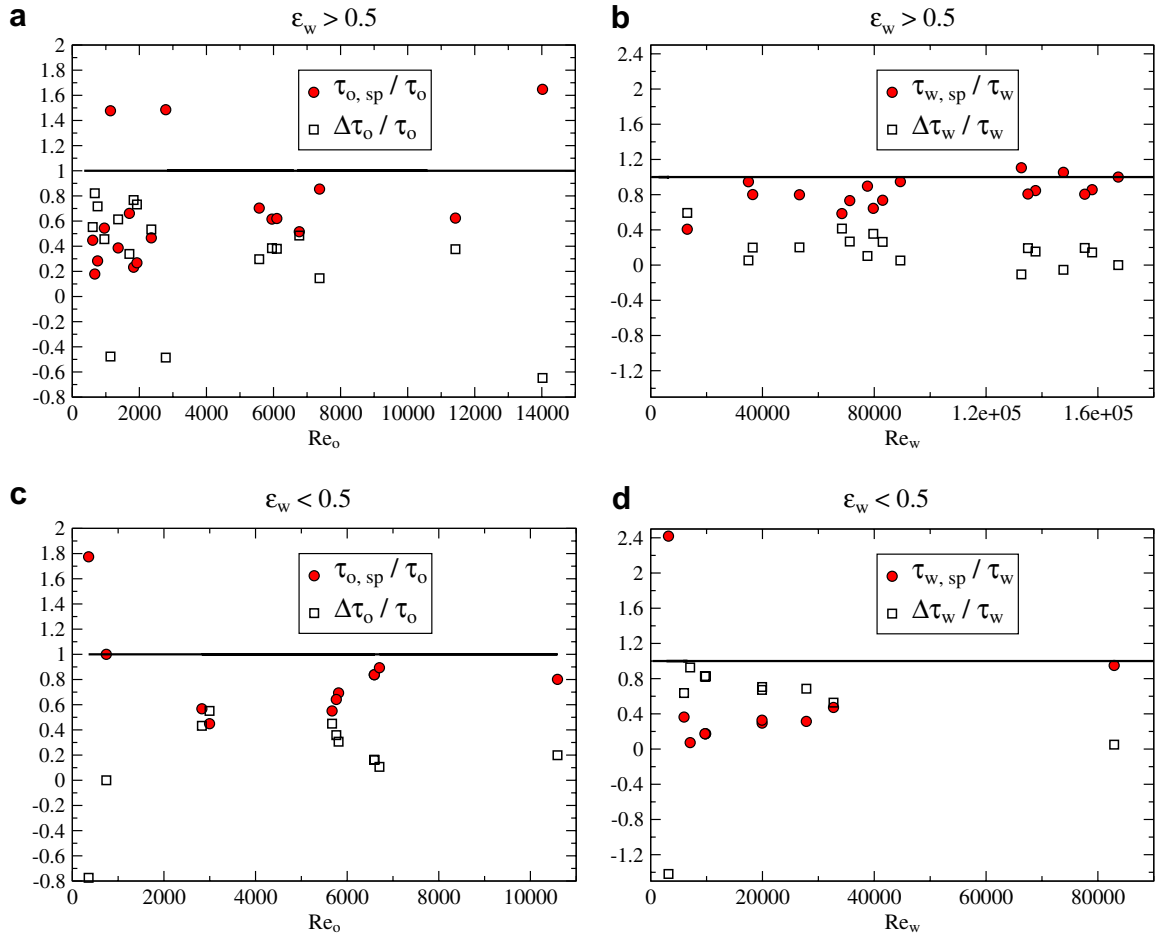

Fig. 5. The wall-shear stresses τ_{sp}, $\Delta\tau$ and τ: (a) the oil side, $\varepsilon_w > 0.5$; (b) the water side, $\varepsilon_w > 0.5$; (c) the oil side, $\varepsilon_w < 0.5$; (d) the water side, $\varepsilon_w < 0.5$.

$\frac{\tau_{sp}}{\tau}$ is larger than 1, which implies a negative value of $\frac{\Delta\tau}{\tau}$ since the sum of the components, normalized by the total wall-shear stress, must be unity. For these points, the total wall-shear stress is reduced compared to the wall-shear stress of the single-phase flow with the same flow parameters.

For both the oil and water phase, there is a critical phase-Reynolds number that determines which component of the total wall-shear stress will dominate. Fig. 5a and c shows the components of the oil wall-shear stress ($\tau_{o,sp}, \Delta\tau_o$), normalized by the total wall-shear stress (τ_o), for the experimental points with $\varepsilon_w > 0.5$ and $\varepsilon_w < 0.5$ respectively. For both sets of the experimental points the critical Reynolds number appeared to be around 4000. All experimental points, except one in both sets, with the oil phase-Reynolds number larger than 4000, have the component $\tau_{o,sp}$ larger than $\Delta\tau_o$. This indicates that the wall-shear stress, for these points, is affected more by the single-phase-like turbulence than by the multi-phase-flow-related phenomena. The oil wall-shear stress of the experimental points with $Re_o < 4000$ is dominated by the $\Delta\tau_o$ component (for some points $\Delta\tau_o$ is even as large as 80% of the total wall-shear stress). For these points, the multi-phase flow related phenomena are more or equally important for determination of the wall-shear stress as the phenomena related to the single-phase flow. There is a trend of a decrease of $\Delta\tau_o$ with an increase of the oil phase-Reynolds number. This trend is more obvious for the experimental points characterised by a thick oil layer at the top ($\varepsilon_w < 0.5$), see Fig. 5c. The decrease of $\Delta\tau_o$ indicates that the influence of multi-phase flow related phenomena over the wall-shear stress is diminishing with increasing phase-Reynolds number.

The critical Reynolds number for the wall-shear stress on the water side appears to be around 35,000, even though it is more difficult to establish one due to the smaller number of the experimental points, especially

those with $\varepsilon_w > 0.5$ and $Re_w < 40{,}000$. However, the wall-shear stress is dominated by $\tau_{w,sp}$ for all of the experimental points with water phase-Reynolds number larger than 35 000. The wall-shear stress component $\Delta\tau_w$ decreases by increasing the water Reynolds number. There is a more obvious trend in distribution of $\Delta\tau$ on the thin water-layer side, see Fig. 5d, than on the thin oil-layer side shown in Fig. 5a. The main difference between these two layers is the level of turbulence. The turbulent fluctuations in the more-viscous-oil layer are strongly suppressed compared to the turbulent fluctuations in the less-viscous-water layer. The different turbulence level, described by the phase-Reynolds number, is probably the main reason for different trends in the distribution of $\Delta\tau/\tau$.

Fig. 6a and b show the total wall-shear stresses normalized by τ_{sp}. The total wall-shear stress is different than 1 only if $\Delta\tau \neq 1$. It can be seen that the wall-shear stress component $\Delta\tau$ of the thicker-phase layer is always smaller than the corresponding $\Delta\tau$ of the thinner-phase layer (the only exception are the points for which the wall-shear stress is reduced compared to the single-phase flow). This means that $\Delta\tau$ depends on the oil–water interface position. The region of the pipe wall closer to the interface is more affected by the interface related phenomena and thus it has higher values of $\Delta\tau$. Fig. 6 also reveals that part of the wall-shear stress caused by the multi-phase flow phenomena ($\Delta\tau$) can be several times higher than the wall-shear stress in the corresponding single-phase flow (τ_{sp}).

Fig. 7 presents the wall-shear stress component $\Delta\tau$ as a function of the phase densimetric Froude number defined as

$$Fr_o = \frac{\rho_o U_o^2}{g\Delta\rho D_{h,o}}, \tag{26}$$

$$Fr_w = \frac{\rho_w U_w^2}{g\Delta\rho D_{h,w}}, \tag{27}$$

where $\Delta\rho$ is the density difference, $D_{h,o}$ and $D_{h,w}$ are the oil- and water-phase hydraulic diameters respectively. The Froude number is the ratio of inertial forces to gravitational forces, and as such can be relevant in describing the instabilities that lead to the occurrence of the interfacial waves (and possibly to entrainment). Gravitational forces tend to keep the interface steady and undisturbed while inertial forces act as the source of instability. Fig. 7a and b reveals that $Fr = 3$ is the critical Froude number for the experimental points with $\varepsilon_w > 0.5$ for both the oil and water phase. There is a local maximum in $\Delta\tau_o/\tau_o$ and $\Delta\tau_w/\tau_w$ at $Fr = 3$ after which $\Delta\tau_o/\tau_o$ and $\Delta\tau_w/\tau_w$ gradually decrease as the Froude number increases. For a Froude number smaller than 3, there is no clear trend in $\Delta\tau_o/\tau_o$ distribution (more than one trend can be noticed). $\Delta\tau_w/\tau_w$ decreases in two points and then reaches a maximum for the lowest Froude number. Similarly, a critical Froude number exists for the experimental points with $\varepsilon_w < 0.5$. However, for these points the critical Froude number differs and it

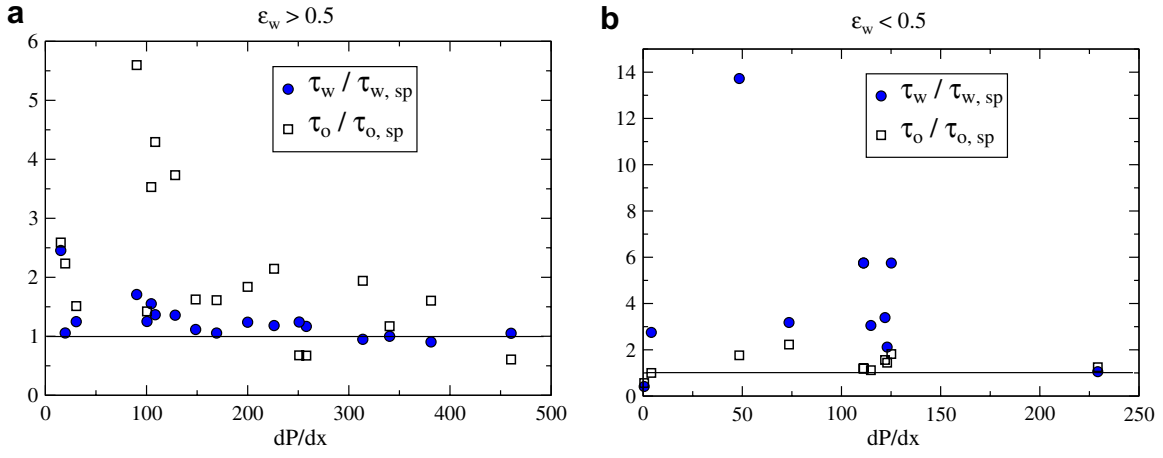

Fig. 6. Total wall-shear stresses at water and oil sides normalized by τ_{sp}: (a) $\varepsilon_w > 0.5$; (b) $\varepsilon_w < 0.5$.

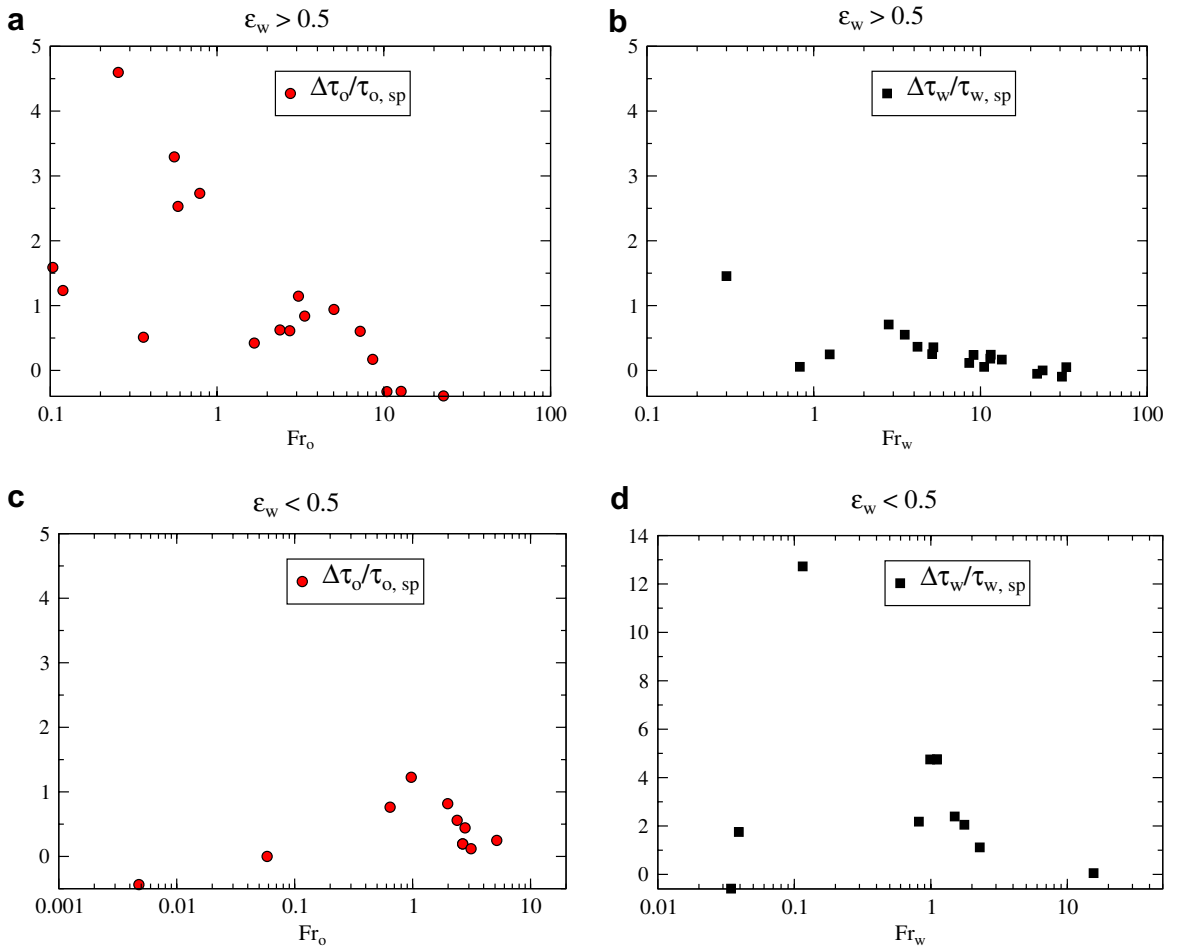

Fig. 7. Component $\Delta\tau$ as function of Froude number: (a) the oil side, $\varepsilon_w > 0.5$; (b) the water side, $\varepsilon_w > 0.5$; (c) the oil side, $\varepsilon_w < 0.5$; (d) the water side, $\varepsilon_w < 0.5$.

appears to be 1 rather than 3. $\Delta\tau_o/\tau_o$ increases with an increase of the Froude number until the critical value is reached ($Fr = 1$) after which $\Delta\tau_o/\tau_o$ gradually decreases toward zero. The same trend exists for $\Delta\tau_w/\tau_w$. The difference between the critical Froude number for the oil–water flow with the thin oil-layer and the thin water-layer is probably caused by the faster growth of the interfacial instabilities with the Froude number[2] for the experimental points with $\varepsilon_w < 0.5$. The thin oil-layer and the thin water-layer of the same thickness and the same velocity have a similar Froude number while their phase-Reynolds numbers differ significantly due to different viscosities. This means that even though the phase-Froude number is similar, the interfacial waves could be very different in frequencies and amplitudes depending on the viscosity of the thinner-layer phase.

The physical picture of the thinner layer is more complex due to the complex interaction of the equally important single-phase and multi-phase flow related phenomena. This could be a reason for the absence of a clear trend in distribution of $\Delta\tau$ for the thinner-layer phase, see Fig. 7a. However, it seems that this interaction is weaker in the thicker-layer flow. Fig. 7b and c show a clear trend in distribution of $\Delta\tau$ on the thicker-layer side. A stable and smooth oil–water interface is more likely to be present for a small Froude number (Smolentsev and Miraghaie, 2005). For this flow condition $\Delta\tau$ is small and $\tau \approx \tau_{sp}$. The increase of the Froude number indicates the growth of the interface instabilities. This leads to the occurrence of the interfacial waves.

[2] The Froude number does not depend on the phase viscosities.

As a result of the wave presence, $\Delta\tau$ increases and reaches its maximum for the critical Froude number. Since the increase of the phase-Froude number is followed by the increase of the phase-Reynolds number, at a certain point the single-phase-flow related wall-shear stress τ_{sp} becomes more dominant than the multi-phase-flow related wall-shear stress $\Delta\tau$. This is a reason for the decrease of $\Delta\tau$ with the further increase of the phase-Froude number.

Some important conclusions can be drawn from the data presented:

- A correlation between the Reynolds number and the wall-shear stress, valid for the single-phase close-to-equilibrium flows, is not well-founded for the oil–water flows in which the interface related phenomena such as interfacial shear, entrainment or interfacial waves, play an important role in the flow dynamics. Consequently, the model for the interfacial-shear stress based on the wall-friction coefficient, for such flow conditions, is also erroneous.
- $\Delta\tau$ has a positive sign, both on the oil and water side, for 90% of the experimental points. This means that the standard closure relations underpredict the wall-shear stress for these points. For approximately 50% of the experimental points, the interfacial shear stress, estimated by closure relation (8), is significantly smaller than the oil and water wall-shear stresses (τ_i is smaller than 25% of the smaller wall-shear stress $\min(\tau_w, \tau_o)$). Although, the interfacial shear stress, calculated by the closure relation, can be erroneous due to the over-simplistic representation of the oil–water interface, the calculation errors that occur for the experimental points with small oil–water velocity differences, are more probably due to erroneous prediction of the wall-shear stress.
- A negative sign of $\Delta\tau$ means that the wall-shear stress is smaller than it would be in the single-phase flow with the same parameters (Re, D_h). The reduction of the wall-shear stress occurs for the flow condition characterised by a thin layer of oil or water at the top or bottom of the pipe, with a phase-Reynolds number smaller than 4000. Postponed transition from the laminar to turbulent regime can be responsible for the wall-shear stress reduction. However, this is not conclusive since some of the points are deep in the laminar regime.
- The wall-shear stress at the thicker-phase-wetted wall always has a smaller contribution coming from $\Delta\tau$ compared to the corresponding wall-shear stress on the thinner-phase-wetted wall. This supports an assumption that $\Delta\tau$ is generated by phenomena related to the existence of the oil–water interface. It also indicates that $\Delta\tau$ depends on the position of the oil–water interface.
- There is a trend of decrease of $\Delta\tau$ with an increase of the phase-Reynolds number. This suggests that the part of the wall-shear stress, caused by the single-phase-like turbulence, becomes more dominant than the component generated by the multi-phase flow related phenomena as the phase-Reynolds number increases.

5. A parametric study of oil–water interface related phenomena

The main difference between a pipe flow in a single-phase regime and a multi-phase stratified flow is the existence of the oil–water interface. It is widely reported that the oil–water interface is stable for a very limited range of sufficiently small phase velocities. As the phase-velocities increase, small amplitude, regular waves develop at the interface. A further increase of the phase velocities leads to a development of irregular, three-dimensional large amplitude roll waves. These waves usually make entrainment of drops, from their crest into the opposite continuous phase, possible. Both entrainment and interfacial waves can have a strong influence on the wall- and interfacial-shear stresses. In addition, the oil–water interface is usually not flat, but more or less curved. All these phenomena, acting alone or in combination, can make the wall-shear stress to differ significantly from the corresponding shear-stress in a single-phase flow with the same Reynolds number. The following parametric studies have been performed in order to investigate the influence of these phenomena on the wall-shear stress and possibilities to represent these phenomena within the two-fluid modelling practice. It was reported by Angeli and Hewitt (2000) and Valle and Kvandal (1995), among others, that the oil–water interface can be strongly curved. However, the preliminary results of the parametric study on the curved interface, using a model proposed by Brauner et al. (1998), showed that the curved interface alone (without taking into account the effect of the thin film on the wall-shear stress) can not explain the main

prediction errors. The focus of the following parametric studies is on drop entrainment and on waviness of the oil–water interface.

5.1. Interfacial waves

The existence of the oil–water interface related phenomena is a possible reason for failure of the two-fluid model to accurately predict the phase velocities. This made the phase-interface physics an interesting research topic that has been widely exploited in the last decades. However, the gas–liquid interface was mainly investigated while very limited research exists on the liquid–liquid interface. A better insight into the wave structures and their interaction with the phase current flows is a necessary pre-requisite for improving the standard two-fluid modelling approach.

The liquid–liquid interface is smooth only for low phase velocities, while the increase of the phase velocities leads to the occurrence of interfacial waves. Depending on the fluid properties and phase velocities, complex, both two- and three-dimensional, wave structures may occur with a wide range of frequencies and amplitudes (Fernandino and Ytrehus, 2006). Large-amplitude roll-waves lead to entrainment of drops into the opposite-phase layer. These waves, whose shape is in fact unknown, can dramatically affect both the interfacial-shear stress, increasing the drag between phases, and the wall-shear stress. Lodahl et al. (1998) investigated the interaction of single-phase oscillatory flow and current in a circular, smooth pipe. They found that, depending on the flow regime, turbulence can be both laminarized (leading to drag reduction) and intensified (increasing the drag). These results are also relevant for the multi-phase-flow research since the existence of the interfacial waves can impose oscillatory flow in the upper and lower fluid layers.

The present parametric study is conducted in order to assess the differences between the wall-shear stress, calculated by closure relation (4), with and without assuming the existence of waves at the oil–water interface. The interfacial waves are approximated by periodic, regular sinusoidal waves with a certain frequency and amplitude, see Fig. 8. In the case of an oscillatory flow, it is important to distinguish between mean and ensemble averaging. The variables (shear-stresses, water and oil hold-ups, phase velocities, etc.) at different cross-sections are assumed to be ensemble-averaged, e.g.

$$\tilde{\phi}(\omega t) = \frac{1}{N_c}\sum_{j=1}^{N_c}\phi[t + (j-1)T], \tag{28}$$

where $\tilde{\phi}$ is the ensemble-averaged variable, ω is the angular frequency of the oscillatory flow, t is time, and N_c is the total number of cycles sampled. The ensemble-averaged variables differ in different cross-sections, e.g. cross-sections I and II, see Fig. 8. The time-averaged variables are defined as the period-averaged values of the corresponding ensemble-averaged values:

$$\overline{\phi} = \frac{1}{T}\int_0^T \tilde{\phi}(\omega t), \tag{29}$$

where T is the period of the oscillatory waves. The time-averaged variables are the same in each cross-section of the domain.

In order to satisfy the continuity equation, the wave velocity C has to be introduced. The coordinate system is attached to the wave and moving by the wave velocity C which means that the wave is stationary while oil and water are moving relative to the wave velocity. Due to the continuity constraint, the phase mass-fluxes are the same in any cross-section, and they are taken to be equal to the mean values from the experiments:

$$(\rho_o(\overline{U}_o - C)\overline{A}_o)_{exp} = \rho_o(\widetilde{U}_o - C)\tilde{A}_o, \tag{30}$$

$$(\rho_w(\overline{U}_w - C)\overline{A}_w)_{exp} = \rho_w(\widetilde{U}_w - C)\tilde{A}_w, \tag{31}$$

where the subscript exp stands for the experimental data. The oil and water velocities $\overline{U}_o$, $\overline{U}_w$, $\widetilde{U}_o$ and $\widetilde{U}_w$ are velocities relative to the pipe wall which means that they can be used for the wall and interfacial shear-stress calculation. The wave velocity can be estimated from the recorded movies only for a few experimental points for which the oil/water interface is clearly visible and waves are more regular, as e.g. in Fig. 9. It appears that

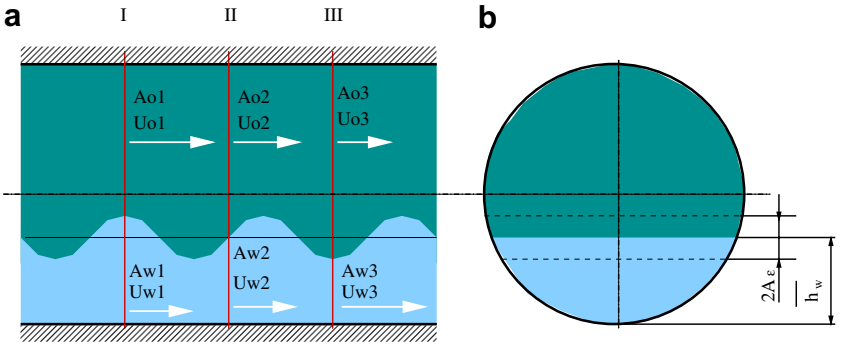

Fig. 8. Schematic diagram of the interface waves: (a) side view, (b) cross-sectional view.

the wave velocity is always between $\overline{U}_o$ and $\overline{U}_w$ (more often closer to the higher velocity). Since no reliable model exists for an accurate estimation of the large amplitude interfacial waves, we roughly estimate the wave velocity by

$$C = \frac{\overline{U}_o + \overline{U}_w}{2}. \tag{32}$$

Now, the water hold-up in any cross-section is defined as

$$\tilde{\varepsilon}_w = \overline{\varepsilon}_w + A_\varepsilon \sin(\omega t), \tag{33}$$

where A_ε is the amplitude of the water-hold-up oscillations. The lower limit for A_ε is 0 while the upper limit is defined by the following expression:

$$A_\varepsilon = \min[\tilde{\varepsilon}_w, (1.0 - \tilde{\varepsilon}_w)]. \tag{34}$$

Eq. (34) allows the ensemble-averaged water hold-up to be equal to 1 (the wave amplitude is equal to the height of the thinner phase layer) or 0 (the waves do not exist) in extreme limits. A finite number of the cross-sections are placed within one wavelength. For each cross-section, the ensemble-averaged cross-section areas $(\tilde{A}_o, \tilde{A}_w)$ are calculated based on the known $\tilde{\varepsilon}_w$, and the ensemble-averaged phase velocities are then calculated from Eqs. (30) and (31). The ensemble-averaged wall-shear stresses can then be calculated along the wall using Eqs. (4) and (5). Finally, the mean-averaged wall-shear stresses are calculated as follows:

$$\overline{\tau}_{wave} = \frac{1}{N_s}\sum_{0}^{N} \tilde{\tau}, \tag{35}$$

where N_s is the number of the cross-sections within the wavelength and $\tilde{\tau}$ is the ensemble-averaged wall-shear stress calculated as

$$\tilde{\tau} = \frac{1}{2}\rho \tilde{f} \tilde{U}^2, \tag{36}$$

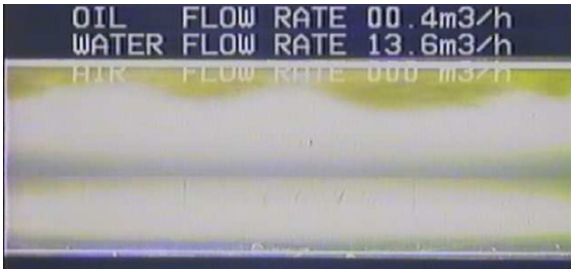

Fig. 9. Picture of the interfacial waves, recorded by Rodriguez and Oliemans (2006).

where $\tilde{f}$ is the ensemble-averaged skin-friction coefficient and $\widetilde{U}$ is the ensemble-averaged phase velocity. For the sake of simplicity, in the following text the over-line (e.q. $\overline{\tau}_{\text{wave}}$), used to denote the mean-averaged variables, is omitted. The wall-shear stress produced by the stratified flow with the smooth, steady interface ($A_\varepsilon = 0$) is defined as

$$\tau(A_{\varepsilon_w} = 0) = \frac{1}{2}\rho\overline{\tilde{f}\widetilde{U}^2}. \tag{37}$$

In this parametric study, we do not solve the two-fluid model equations but search for the value of A_ε that produces the minimal deviation between the oil and water mean-wall-shear stresses and the corresponding shear stresses found to satisfy the two-fluid equations when experimental data are imposed (calculated in Section 4). The shear stress deviation is defined as

$$\text{dev} = \frac{|\tau_o - \tau_{o,\text{wave}}|}{\tau_o} + \frac{|\tau_w - \tau_{w,wave}|}{\tau_w}, \tag{38}$$

where τ_o and τ_w are the oil and water wall-shear stresses determined by the parametric study in Section 4. In the adopted equations, the wave frequency does not play a role in the determination of the wall-shear stresses. However, it has been experimentally confirmed that the wave frequency determines the way in which the current flow interacts with the waves (Lodahl et al., 1998).

Fig. 10a and b show comparisons between the wall-shear stresses that satisfied the two-fluid-model equations (τ_o and τ_w), and the wall-shear stresses $\tau_{o,\text{wave}}$ and $\tau_{w,\text{wave}}$, calculated by Eq. (35) for the experimental points with $\varepsilon_w > 0.5$. In parallel, τ_o and τ_w are compared with the wall-shear stresses calculated by Eq. (35), with an assumption of smooth, steady interface ($A_\varepsilon = 0$). Fig. 10a shows the wall-shear-stress errors on the oil side. The errors can be as high as 80% when a smooth interface is assumed. If the wavy oil–water interface is considered, the shear-stress errors can be significantly reduced for all of the experimental points except for those points for which the wall-shear stress is found to be smaller than the corresponding shear stress of the single-phase flow (the error for these points has a negative sign). The reduction of the wall-shear stress cannot be predicted by the existing closure relations.

The wall-shear-stress errors for the water-wetted wall, shown in Fig. 10b, are also reduced for most of the experimental points even though not so significantly as on the oil side. It is realistic that the interfacial waves influence more strongly the wall-shear stress on the thinner-layer side (the oil layer in this case) than the wall-shear stress on the thicker(water)-layer side.

The wave amplitudes that minimize the error, defined by Eq. (38), are shown in Fig. 10c and d. Both figures show the same wave amplitudes but relative to different phase-layer thicknesses. The amplitude values cannot be experimentally confirmed and should be taken with caution. Moreover, the wave velocity, which is roughly estimated, can strongly influence the predicted amplitude values. However, the recorded movies of the oil–water flow, made by Rodriguez and Oliemans (2006), reveal that the predicted values of the interfacial-wave amplitudes are not unrealistic, at least for some of the experimental points. The amplitudes predicted by this parametric study, are amplitudes of those waves that can influence the wall-shear stress calculated by Eq. (36). These amplitudes do not necessarily correspond to the amplitudes of real, physical interfacial waves.

Fig. 11 shows the results for the experimental points for which water forms a thinner layer at the bottom of the pipe ($\varepsilon_w < 0.5$). The trends are similar to those previously observed. The calculation of the wall-shear stress, wetted by the thinner layer, is strongly affected if the presence of the large-amplitude waves is assumed, see Fig. 11b. The water shear-stress error can be significantly reduced if the interfacial waves are considered. The wall-shear stress on the oil (thicker) side is less affected by the waves, see Fig. 11a. The resulting wave amplitudes are shown in Fig. 11c and d. The present parametric study suggests that only the high amplitude waves have a significant influence on the wall-shear stress.

This parametric study shows that the mean-flow-rates can produce a rather different value of the wall-shear stress modelled by Eq. (4), depending on the assumption for the state of the oil–water interface. For most of the experimental points, the prediction of the wall-shear stress is improved if interfacial waves of certain amplitude, are assumed. The consideration of the interfacial waves can offer an explanation for the significant difference between the wall-shear stress values in single-phase and multi-phase flows. Lodahl et al. (1998)

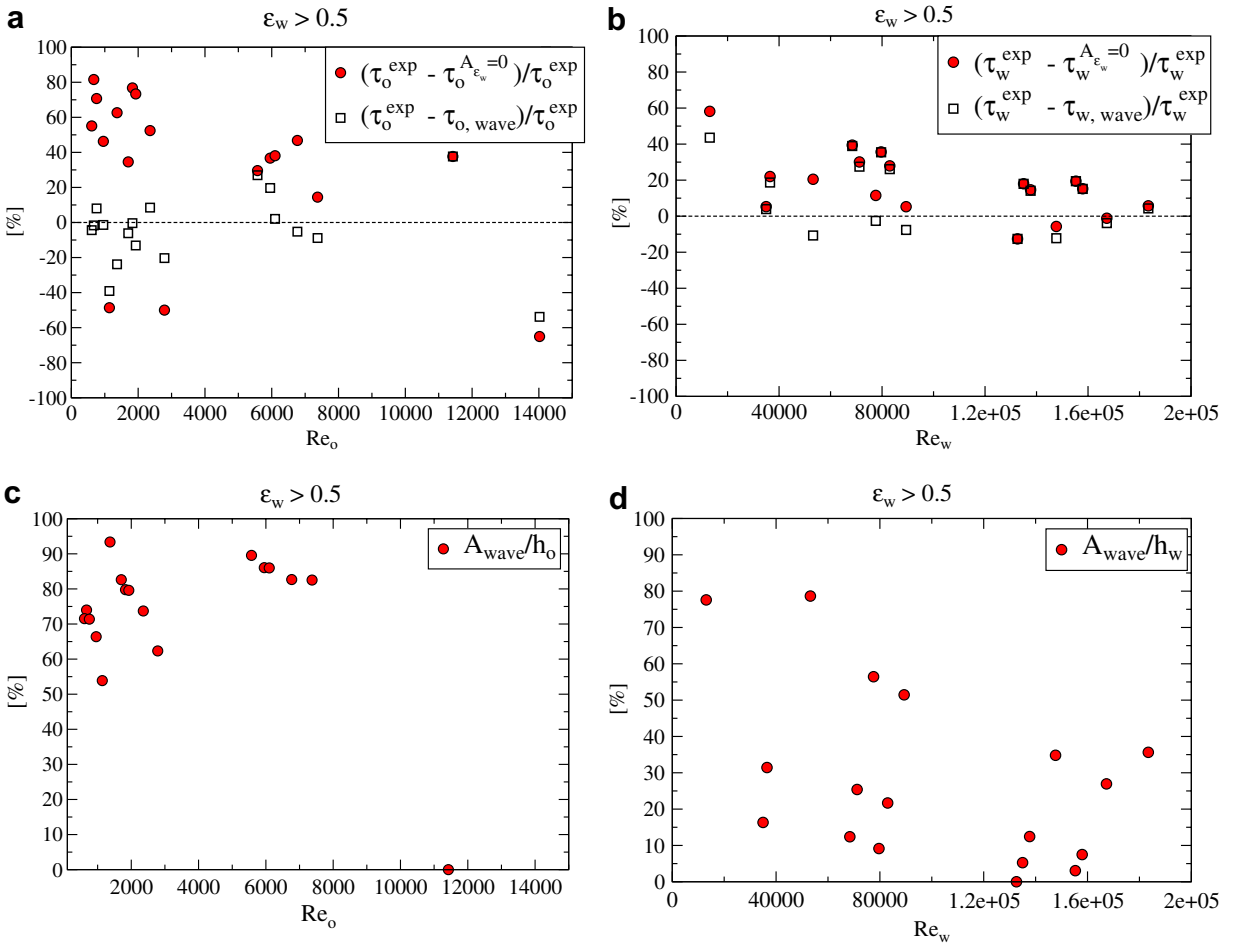

Fig. 10. (a) Comparison of $\tau_{o,wave}$ and $\tau_{o,st}$ with τ_o for $\varepsilon_w > 0.5$; (b) comparison of $\tau_{w,wave}$ and $\tau_{w,st}$ with τ_w for $\varepsilon_w > 0.5$; (c) the wave amplitude relative to the oil-layer thickness for $\varepsilon_w < 0.5$; (d) the wave amplitude relative to the water-layer thickness for $\varepsilon_w < 0.5$.

found that the transition to turbulence, that occurs at $Re \approx 2000$ for a current flow, is delayed by superimposing an oscillatory flow on the current. The flow becomes turbulent only after Re reaches a value of about 7500 in the case of the combined (current and oscillatory) flow. They found that the suppression of turbulence occurs if the flow is wave-dominated with the oscillatory component of the flow in the laminar regime. On the other hand, the wall-shear stress increases, compared to the pure current regime, if the flow becomes wave-dominated with the oscillatory boundary layer in the turbulent regime. It was shown that the wall-shear stress can be as high as four times the wall-shear stress of the pure current. Interestingly, the wall-shear stress stays unchanged, compared to the pure current values, as long as the flow remains current-dominated, even if the oscillatory boundary layer is in the turbulent regime.

The results from the parametric study, presented in Section 4, show that the wall-shear-stress reduction occurs when the phase-Reynolds number is in the laminar or low-Reynolds number regimes. The phase-Reynolds number is between $1000 < Re < 3000$ for all but one of the experimental points for which the wall-shear stress is reduced compared to the single-phase flow. The experimental points for which the wall-shear stress is reduced, are characterised by small phase-velocities. It is likely that the small phase-velocity will produce an oscillatory flow with a laminar regime, which is a necessary pre-requisite for the suppression of turbulence, according to Lodahl et al. The present parametric study reveals that the flow regimes for which the wall-shear stress is strongly affected by the presence of the interfacial waves are characterised by a moderate phase-Reynolds number (the phase-Reynolds numbers that are significantly smaller than the maximum phase-Reynolds

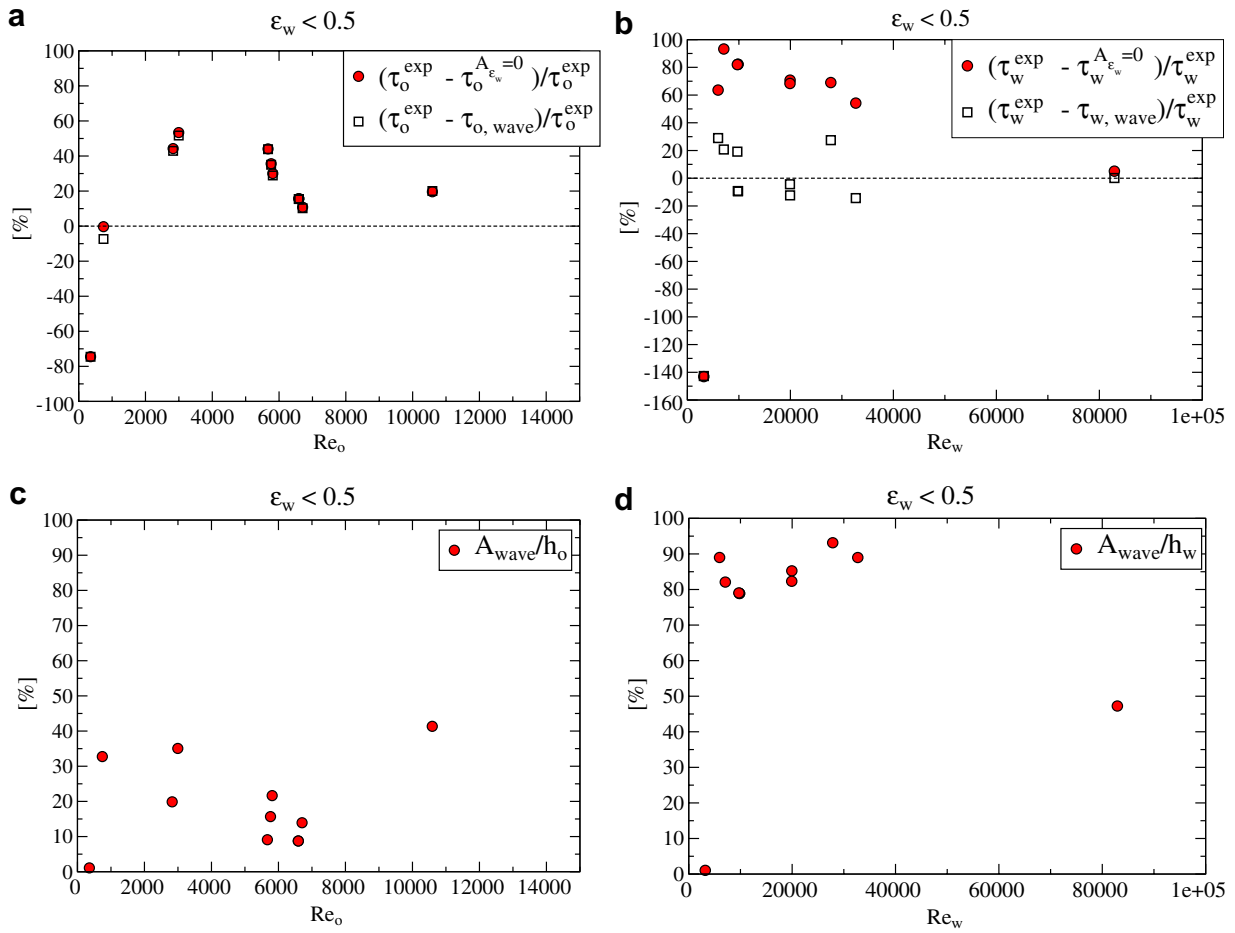

Fig. 11. (a) Comparison of $\tau_{o,wave}$ and $\tau_{o,st}$ with τ_o for $\varepsilon_w < 0.5$; (b) comparison of $\tau_{w,wave}$ and $\tau_{w,st}$ with τ_w for $\varepsilon_w < 0.5$; (c) the wave amplitude relative to the oil-layer thickness for $\varepsilon_w < 0.5$; (d) the wave amplitude relative to the water-layer thickness for $\varepsilon_w < 0.5$.

number for which the flow pattern is still classified as stratified) and interfacial waves with the high wave amplitudes. For such a flow, it is possible that the oscillatory Reynolds number is larger than the phase-Reynolds number. This is a condition in which the wall-shear stress is larger than the wall-shear stress of the pure current, according to Lodahl et al. Finally, the Reynolds number of the oscillatory flow simply cannot follow the Reynolds number of the current since the wave amplitude is confined by the thinner-layer height, and the flow inevitably becomes current dominated. This could explain the trend of the error reduction with increase of the phase-Reynolds number noticed in Section 3.2. The part of the wall-shear stress induced by the oscillatory flow then becomes negligible compared to the total wall-shear stress as the phase-layers become highly turbulent.

5.2. Drop entrainment

Fig. 12a and b schematically describe two flow patterns: stratified flow, where no mixing of the phases occurs at the interface and dual continuous flow, where droplets of the opposite phase exist in the upper and lower layers. Entrainment of one phase into the other occurs when the interfacial-shear stress becomes sufficiently high to drag part of the fluid into the continuous layer of the opposite phase. The high-amplitude interfacial waves can create a condition for entrainment occurrence since the drag between phases increases rapidly at the crest of the waves.

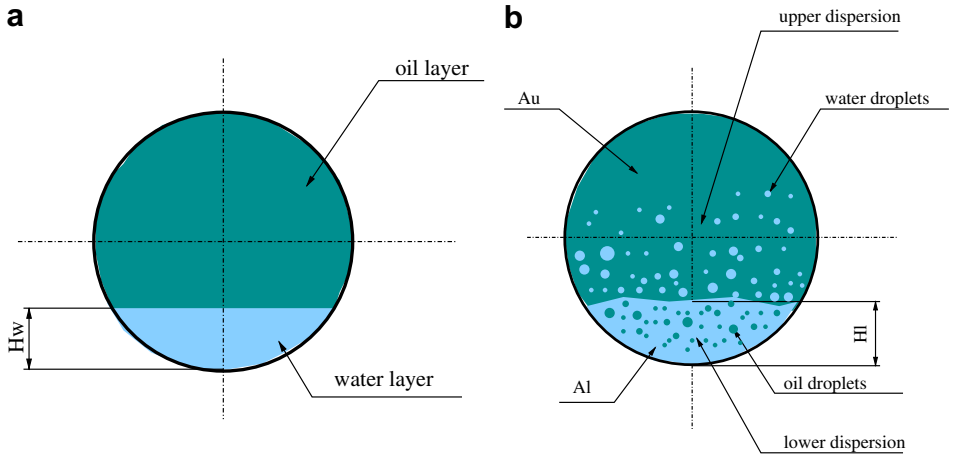

Fig. 12. Schematic description of (a) stratified flow without drop entrainment; (b) stratified flow with drop entrainment.

The common name for the flow patterns where both phases form continuous layers at the top and bottom of the pipe respectively, with the presence of dispersed drops of the opposite phase at various concentrations, is dual continuous flow. Angeli and Hewitt (2000) reported on a three layer flow pattern, which was observed for mixture velocities of 0.7–1.3 m/s and water volume fractions of 0.3–0.5. This flow pattern has two distinct layers of oil and water at the top and bottom of the pipe, respectively with a layer of drops around the interface. Stratified flow with mixing at the interface (ST&MI) was observed at approximately the same mixture velocities as the three layer flow and at water volume fractions below 0.3 and above 0.5.

Lovick and Angeli (2004) have performed detailed studies of the dual continuous flow pattern in oil–water flows. They observed entrainment of phases at lowest 0.8 m/s mixture velocity and up to 3 m/s mixture velocity. It was found that at the lower mixture velocities, the drops are mainly concentrated around the phase interface, while at higher mixture velocities, the dispersed phase increases and extends towards the pipe wall.

5.2.1. Two-dispersion model (TDM)

Two different routes for entrainment representation, within two-fluid modelling, have been explored. In the first route, we assume that the entrained drops form a stable dispersion in the upper and lower stratified layers. We denote this approach as the two-dispersion model. In reality this condition might occur if the inertia forces in the continuous layer are sufficient to overcome buoyancy forces that tend to drag the entrained drops back to the layer of origin. The entrainment parameters, in this approach, are defined as

$$E_o = \frac{A_{o\_droplets}}{A_o}, \tag{39}$$

$$E_w = \frac{A_{w\_droplets}}{A_w}, \tag{40}$$

where $A_{o\_droplets}$ and $A_{w\_droplets}$ are areas covered by the oil droplets in the water continuous phase and the water droplets in the oil continuous phase, respectively. It is obvious that the heights of the upper and lower layers (H_l and H_u), the upper and lower cross-sectional areas (A_u, A_l), and the wetted perimeter (S_u, S_l and S_i) depend on the amount of drops that entrains into the opposite layer.

The lower and upper cross-section areas are calculated as follows:

$$A_l = A_w(1.0 - E_w) + A_o E_o, \tag{41}$$

$$A_u = A_o(1.0 - E_o) + A_w E_w, \tag{42}$$

where the subscripts o and w refer to oil and water respectively. The oil and water cross-section areas (A_o and A_w) are calculated from the water hold-up. Knowing the entrainment parameters, the flow geometry can be calculated.

If we assume that the entrained drops have the same velocity as the continuous layer, the mixture densities of the upper and lower layers are defined as

$$\rho_l = \frac{\rho_o A_o E_o + \rho_w A_w (1 - E_w)}{A_l}, \tag{43}$$

$$\rho_u = \frac{\rho_w A_w E_w + \rho_o A_o (1 - E_o)}{A_u}. \tag{44}$$

The mass balances on the oil and water read:

$$U_{os} A = U_u (A_u - A_w E_w) + U_l A_o E_o, \tag{45}$$

$$U_{ws} A = U_l (A_l - A_o E_o) + U_u A_w E_w. \tag{46}$$

These two equations define the in situ velocities in the upper and lower layers (U_u and U_l) in terms of the hold-ups and input flow-rates. The superficial velocities of the lower and upper layers can be derived from Eqs. (45) and (46):

$$U_{us} = \frac{A_l U_{os} - E_o A_o (U_{os} + U_{ws})}{A_l - E_o A_o - \frac{E_w A_w A_l}{A_u}}, \tag{47}$$

$$U_{ls} = \frac{A_u U_{ws} - E_w A_w (U_{ws} + U_{os})}{A_u - E_w A_w - \frac{E_o A_o A_u}{A_l}}. \tag{48}$$

The mixture viscosities of the upper and lower phases are calculated as described in Section 2.2. Here, the water hold-ups in the upper and lower layers are defined as

$$\varepsilon_{wu} = \frac{A_w E_w}{A_u}, \tag{49}$$

$$\varepsilon_{wl} = \frac{A_w (1 - E_w)}{A_l}. \tag{50}$$

The upper and lower layers can be treated both as water-in-oil and oil-in-water dispersions, depending on the critical water cut. In extreme limits, $E_o \to 0$ and $E_w \to 1$ or $E_o \to 1$ and $E_w \to 0$, the solution of the homogeneous model is restored.

Since no entrainment model exists, the entrainment parameters need to be pre-defined. In the current study, the oil and water entrainment parameters are gradually increased from 0 to 1. The superficial velocities are calculated for finite combinations of the oil and water entrainment parameters (the entrainment parameters are gradually increased with some small step values). The resulting entrainment values are then those that produce a minimal prediction error. Even though the existence of interfacial waves are a necessary pre-requisite for entrainment to occur, the influence of the wavy interface on the wall- and interfacial-shear stresses is not taken into account for the sake of simplicity. The aim of this parametric study is to investigate the influence of entrainment terms in the two-fluid model on the model accuracy. However, at this point the values of the entrainment parameters thus found cannot be experimentally confirmed and need to be taken with caution.

It is realistic to assume that entrainment of one phase into the other exists for the experimental points with the ST&MI and Do/w & w flow patterns. Fig. 13 shows a comparison between the model results and the experimental data. Fig. 13a and c present results for the experimental points with water hold-up larger than 0.5, while Fig. 13b and d shows results for the points with $\varepsilon_w < 0.5$. As it can be seen in Fig. 13, there are points for which it is possible to find E_o and E_w values that significantly reduce the prediction errors for U_{os} and U_{ws}. For the experimental points with $\varepsilon_w > 0.5$, the average error for the oil superficial velocities reduces from 55% to 27%, while the maximum deviation decreases from 195% to 77%. The water superficial velocities are improved for most of the experimental points, see Fig. 13c. However, the velocities for four points are significantly overpredicted compared to both the experimental values and the two-fluid model results. It is interesting to notice that these four points all belong to ST&MI and have rather similar flow parameters ($95 < \frac{dp}{dx}[\mathrm{Pa/m}] < 129$ and $0.75 < \varepsilon_w < 0.9$). Furthermore, the maximum deviation for the water superficial velocity is 15.5%, if these four points are excluded. This might indicate that the flow condition of these points

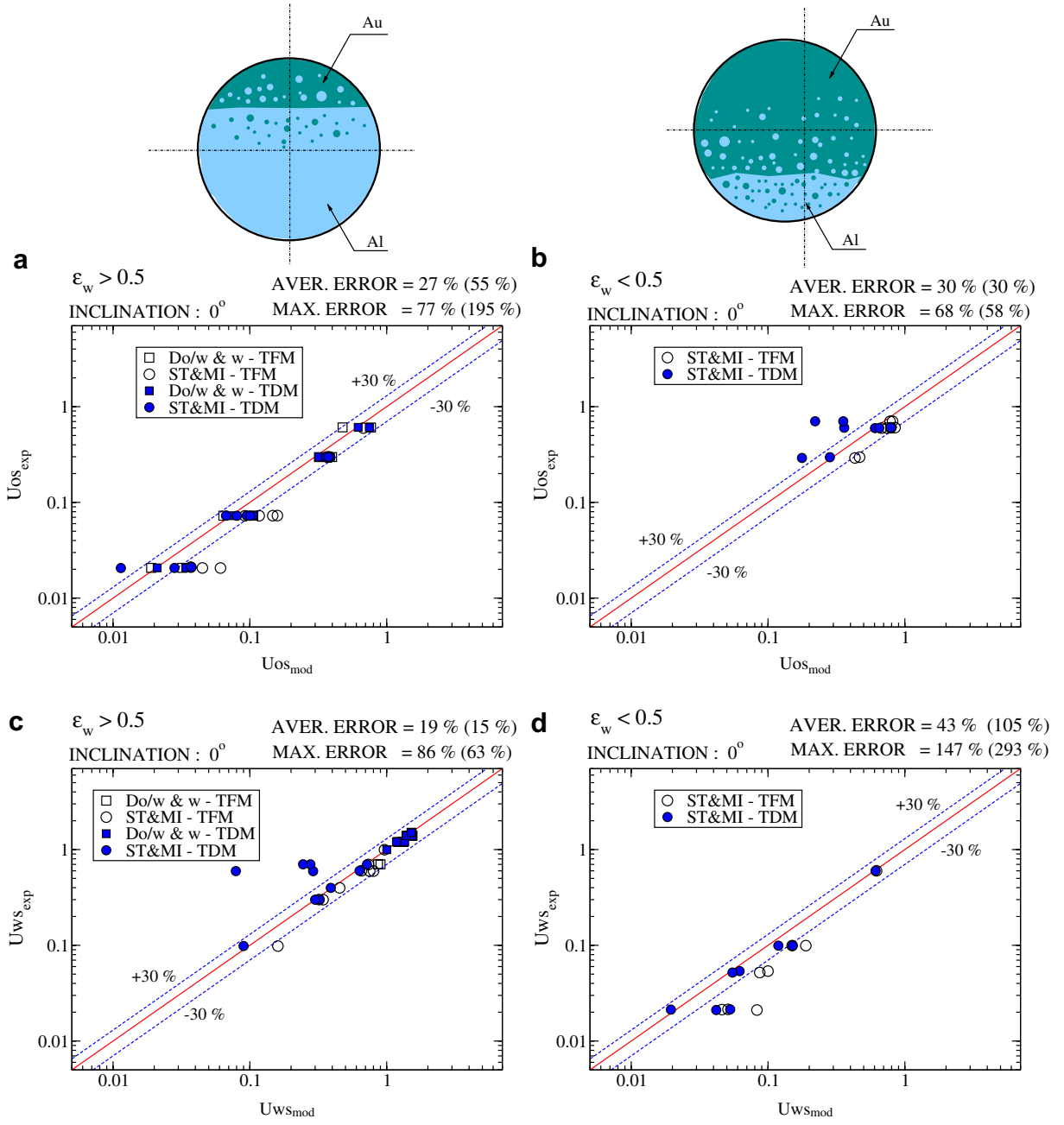

Fig. 13. Comparison of the two-dispersed model (TDM) results with the experimental data: (a) U_{os} for the exp. points with $\varepsilon_w > 0.5$; (b) U_{os} for the exp. points with $\varepsilon_w < 0.5$; (c) U_{ws} for the exp. points with $\varepsilon_w > 0.5$; (d) U_{ws} for the exp. points with $\varepsilon_w < 0.5$.

is closer to a fully stratified flow than to the dual continuous flow. In that case the interfacial waves are more likely to cause the large prediction error of the oil velocity than the drop entrainment.

Generally, the TDM results for U_{os} are more significantly influenced, compared to the two-fluid-model results, than the results for U_{ws}. This is not unexpected since the water-wetted wall is relatively far from the interface and thus less affected by entrainment of oil. Lovick and Angeli (2004) observed that the size and number of drops dispersed in the continuous phase decreases, as the distance from the interface increases. It is interesting to notice that the averaged and maximum prediction errors for U_{ws}, predicted by the standard

two-fluid model for the experimental points with $\varepsilon_w > 0.5$, are significantly smaller than those for the corresponding oil layer. The flow patterns are predicted with a similar accuracy (67%) as for the two-fluid model.

The resulting entrainment parameters are shown in Fig. 14a. Fig. 14c shows which phase entrains more into the opposite layer (e.g. $A_{o\_droplets}/A = E_o\varepsilon_o$). From this figure, it can be seen that the entrainment of oil droplets in the water zone is higher than the entrainment of the water droplets in the oil zone, for most of the experimental points. This is in line with the experimental findings of Valle and Kvandal (1995). However, the entrainment fractions they found (defined as in Fig. 14c and d) have a maximal value of 0.1. Although the oil and water properties in the Valle and Kvandal (1995) experiments differ from those used in the experiments of Rodriguez and Oliemans, this might indicate that some of the resulting oil and water entrainment param-

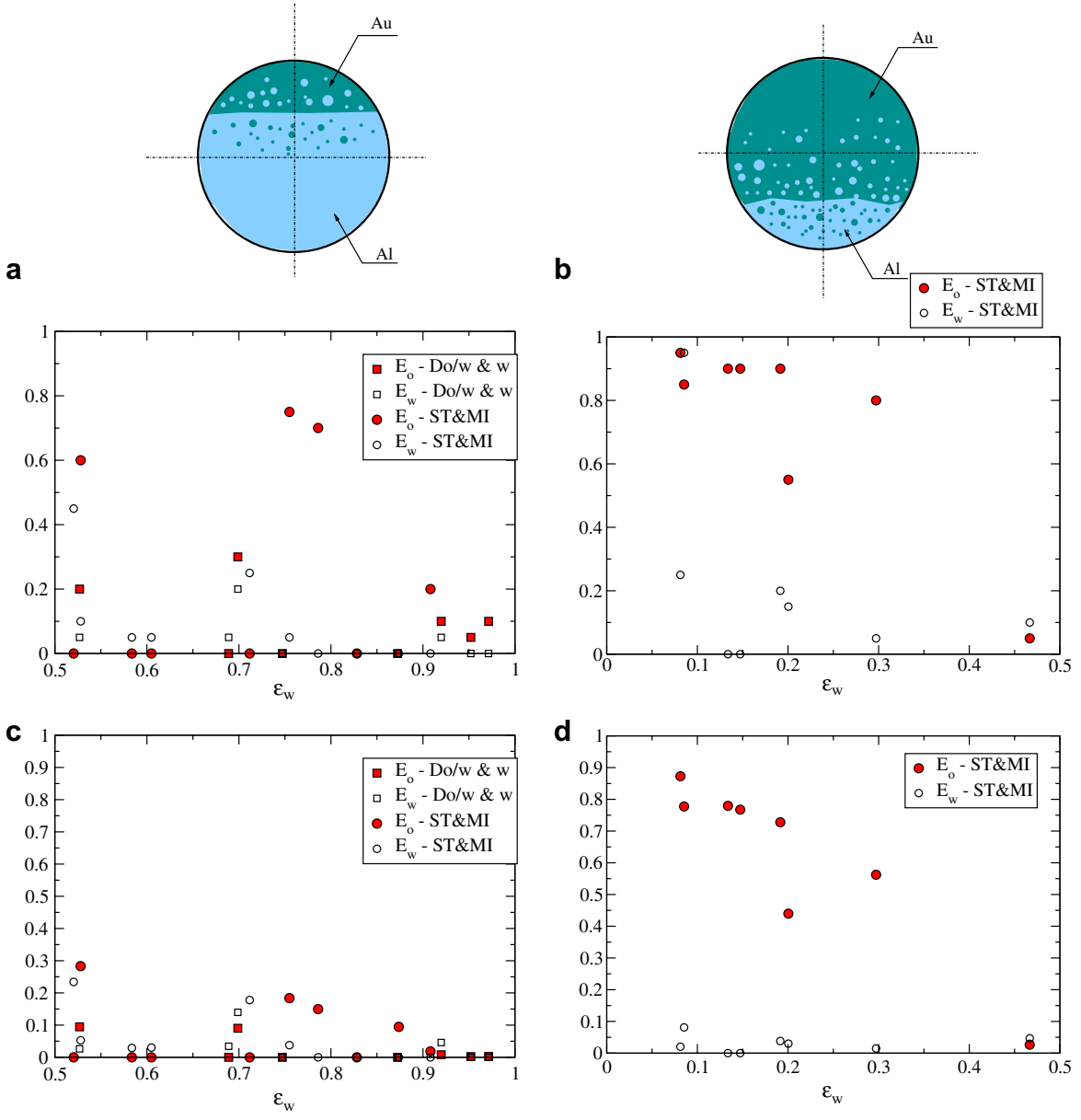

Fig. 14. Resulting entrainment parameters: (a) E_o and E_w for the exp. points with $\varepsilon_w > 0.5$; (b) E_o and E_w for the exp. points with $\varepsilon_w < 0.5$; (c) $E_o\varepsilon_o$ and $E_w\varepsilon_w$ for the exp. points with $\varepsilon_w > 0.5$; (d) $E_o\varepsilon_o$ and $E_w\varepsilon_w$ for the exp. points with $\varepsilon_w < 0.5$.

eters are not realistic. It is indicative that all points with the Do/w & w flow pattern have E_o and E_w close to the values found by Valle and Kvandal while the points denoted as ST&MI have higher values of E_o and E_w.

The results for the experimental points with water hold-up smaller than 0.5 reveal that, for these points, the stable dispersions in the upper and lower layers probable do not exists. While both averaged and maximal prediction errors for the water superficial velocity are significantly reduced, the oil superficial velocities are overpredicted for almost all points. The resulting water and oil entrainment parameters, shown in Fig. 14b and d, are not realistic. The oil entrainment parameters are very high for almost all experimental points. This implies that all of the oil is entrained into the lower layer, creating oil continuous flow. The experimental observation confirms that this scenario is not possible.

5.2.2. Two-fluid model with entrainment (TFE)

In the second approach, we assume that entrained drops exchange momentum with the continuous layer after which they are forced back to the layer of origin due to the buoyancy forces. In order to use the mean-averaged water hold-up for calculation of the water-layer height, the entrainment rate has to be equal to the rate of deposition of the entrained drops. This scenario is likely to occur when the oil and water velocities are relatively small, so the inertia forces are not strong enough to overcome the buoyancy forces that tend to re-establish the fully stratified condition.

If we consider the water and oil layers, shown in Fig. 15, to be two control volumes, the convection terms in the momentum equations are defined as follows:

$$\int \rho_w U_w U_{w,j}\,\mathrm{d}S_j = -\dot{m}_w U_w + \dot{m}_w U_w + \dot{E}_w U_w - \dot{E}_o U_o - \dot{E}_w U_o + \dot{E}_o U_w = (U_w - U_o)(\dot{E}_w + \dot{E}_o), \tag{51}$$

$$\int \rho_o U_o U_{o,j}\,\mathrm{d}S_j = -\dot{m}_o U_o + \dot{m}_o U_o + \dot{E}_o U_o - \dot{E}_w U_w - \dot{E}_o U_w + \dot{E}_w U_o = -(U_w - U_o)(\dot{E}_w + \dot{E}_o), \tag{52}$$

where j denotes a control-volume-face value, $\dot{m}_o$ and $\dot{m}_w$ are the oil and water mass fluxes respectively, $\dot{E}_o$ and $\dot{E}_w$ are the oil and water entrainment rates respectively. The first two terms in the LHS of Eqs. (51) and (52) are convective transport of momentum through the left and right control volume boundaries. Terms with $\dot{E}_o$ and $\dot{E}_w$ represent convective transport of momentum through the interface boundary due to the oil and water drop entrainment respectively. The sign of these terms depends on whether drops are entering or leaving the continuous layer. It is assumed that the drop entrains into the opposite layer with the axial velocity equal to the axial velocity of the layer of origin. In the moment of deposition, the drop axial velocity is equal to the axial velocity of the host layer. From Eqs. (51) and (52), it follows that the entrainment rates are defined as

$$\dot{E}_o = \underbrace{\rho_o V_o S_i}_{\dot{e}_o} L, \tag{53}$$

$$\dot{E}_w = \underbrace{\rho_w V_w S_i}_{\dot{e}_w} L, \tag{54}$$

where V_o and V_w are the wall-normal velocities of the oil and water drops at the oil–water interface respectively, L is the pipe length and $\dot{E}_o$ and $\dot{e}_w$ are the oil and water specific entrainment rates respectively. The momentum equations for the water and oil phases now read:

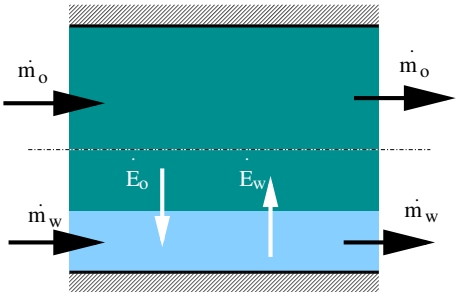

Fig. 15. Schematic description of the drop entrainment.

$$-\frac{\mathrm{d}P}{\mathrm{d}x}+\tau_{\mathrm{o}}\frac{S_{\mathrm{o}}}{A_{\mathrm{o}}}\pm\tau_{\mathrm{i}}\frac{S_{\mathrm{i}}}{A_{\mathrm{o}}}+\rho_{\mathrm{o}}g\sin\alpha-\frac{1}{A_{\mathrm{o}}}(U_{\mathrm{w}}-U_{\mathrm{o}})(\dot{e}_{\mathrm{w}}+\dot{e}_{\mathrm{o}})=0, \tag{55}$$

$$-\frac{\mathrm{d}P}{\mathrm{d}x}+\tau_{\mathrm{w}}\frac{S_{\mathrm{w}}}{A_{\mathrm{w}}}\mp\tau_{\mathrm{i}}\frac{S_{\mathrm{i}}}{A_{\mathrm{w}}}+\rho_{\mathrm{w}}g\sin\alpha+\frac{1}{A_{\mathrm{w}}}(U_{\mathrm{w}}-U_{\mathrm{o}})(\dot{e}_{\mathrm{w}}+\dot{e}_{\mathrm{o}})=0. \tag{56}$$

The new term in the oil and water momentum equations is a redistributive term, which represents the transfer of momentum from one phase to the other and vice-versa. The transport of momentum across the interface is a function of the phase-velocity difference. This is physically well founded since the entrainment is a consequence of the sufficiently large interfacial-shear stress. Thus, the entrainment term can be expressed as function of the interfacial-shear stress that is defined by Eq. (8).

In this parametric study, the oil and water entrainment rates $\dot{e}_{\mathrm{o}}$ and $\dot{e}_{\mathrm{w}}$ are parameters. The resulting entrainment parameters are those that minimize the velocity prediction error, compared to the experimental results. Fig. 16a and b present the resulting superficial velocities for the experimental points for which the water hold-up is larger than 0.5. The standard two-fluid model overpredicts the oil superficial velocity while the water superficial velocity is relatively well predicted. The two-fluid model with entrainment significantly

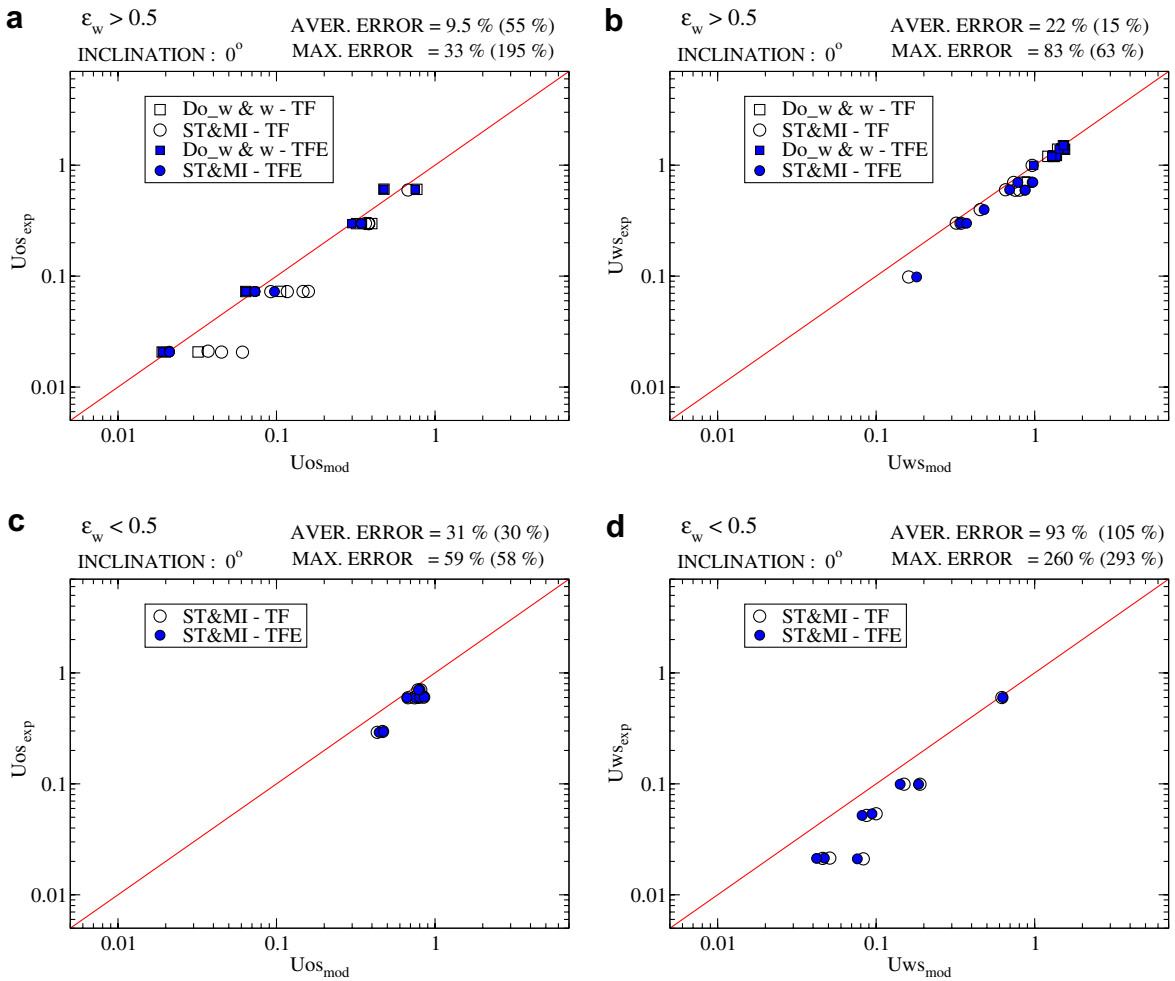

Fig. 16. Comparison of the superficial-velocity results obtained by the two-fluid model with entrainment (TFE) with the experimental data: (a) U_{os} for the exp. points with $\varepsilon_{\mathrm{w}} > 0.5$; (b) U_{ws} for the exp. points with $\varepsilon_{\mathrm{w}} > 0.5$; (c) U_{os} for the exp. points with $\varepsilon_{\mathrm{w}} < 0.5$; (d) U_{ws} for the exp. points with $\varepsilon_{\mathrm{w}} < 0.5$.

improves the prediction of the oil velocity, while the prediction of the water velocity becomes less accurate with the averaged error of 15% increasing to 22%. This is expected since the entrainment term in the momentum equations redistributes the available momentum between the phases. It was shown in Section 4 that the standard two-fluid model underpredicts the wall-shear stress on both water and oil side for most of the experimental points. This implies that the redistribution of the phase momentums can only be beneficial for the lower-velocity phase.

The results for the second set of the experimental data ($\varepsilon_w < 0.5$) are shown in Fig. 16c and d. Here, there is no significant change in the superficial velocities results, neither for the oil or water phase, compared to the values obtained with the standard two-fluid model. This suggests that for these points drop entrainment has a minor effect on the wall-shear stress.

Fig. 17a and b present the entrainment rates normalized by the corresponding phase and total mass-flow rate, respectively. The maximum entrainment rate that occurs is around 12% or 8%, depending on the normalization variable. The resulting entrainment rates are in the same range as those found by Valle and Kvandal (1995). The thicker layer phase entrains more into the thinner layer than opposite. This is in line with the experimental findings of Valle and Kvandal (1995). The highest water entrainment rates occur around $h_w/D \approx 0.7$, while a trend of the oil entrainment-rate distribution is not so clear. The distribution of the entrainment rates shows that more entrainment occurs for the points with $h_w/D > 0.5$. Neither, the two-dispersion model nor the two-fluid model with entrainment, predicts the superficial velocities significantly better for the experimental points with $\varepsilon_w < 0.5$, compared to the results obtained with the standard two-fluid model. This leads us to conclude that the high prediction errors for the experimental points with $\varepsilon_w < 0.5$ cannot be explained by entrainment, or at least not by entrainment alone.

As mentioned earlier, the flow dynamics of the oil–water flow with a thin layer of oil or a thin layer of water can be rather different due to the different fluid properties. Both parametric studies, with the two-dispersion model and two-fluid model with entrainment, suggest that the flow dynamics of the oil–water flow significantly differs depending on the fluid properties of the thin layer. This still has to be confirmed experimentally. Fig. 18a shows that the differences between the oil and water Reynolds numbers are significant for the experimental points with $\varepsilon_w > 0.5$. For these points, the more viscous phase (oil) flows in the thin layer at the top, which implies a smaller Reynolds number compared to the Reynolds number of the water phase.

However, the differences between the oil and water Reynolds numbers are not so high for the experimental points with $\varepsilon_w < 0.5$, see Fig. 18b. Now, the less viscous phase (water) flows in the thin layer at the bottom. Due to the different viscosities, the differences between the phase-velocities are significantly higher when oil forms a thin layer at the top than the other way around. This may have a profound impact on the flow dynamics since both interfacial waves and entrainment are strongly influenced by the phase-velocity difference.

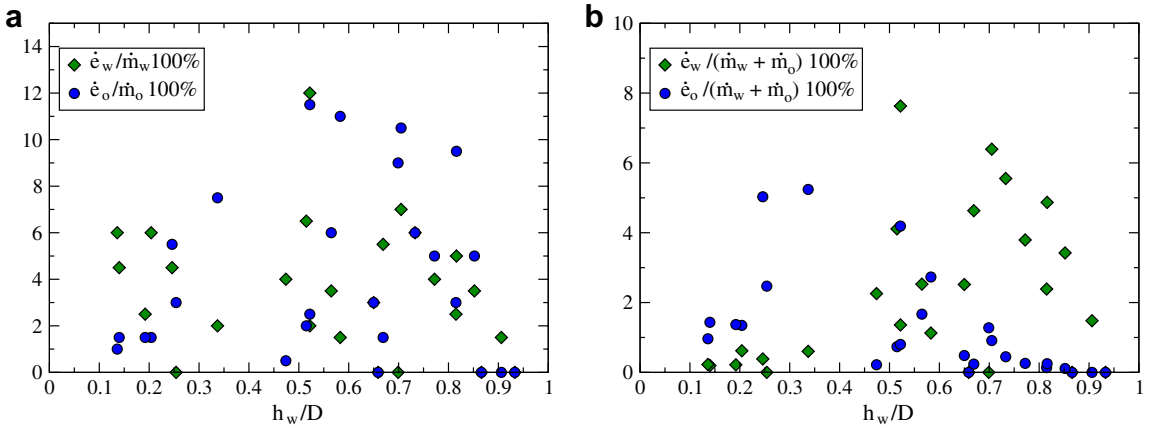

Fig. 17. The entrainment rates found to minimize the prediction errors: (a) normalized by the phase mass-flux, (b) normalized by the total mass-flux.

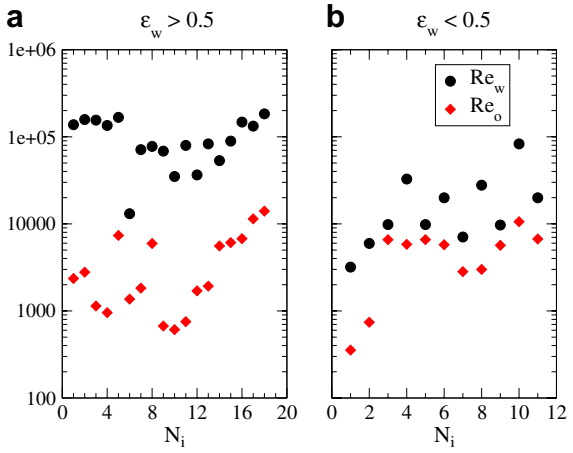

Fig. 18. The phase-Reynolds number for the experimental points: (a) $\varepsilon > 0.5$; (b) $\varepsilon < 0.5$.

6. Conclusions

The two-fluid model, traditionally used for predicting the pressure drop and water hold-up, is used to calculate the superficial velocities in horizontal oil–water flow. The highest prediction errors, for both the standard and inverse calculations, are present for the experimental points in stratified regions characterised by low or high values of the water hold-ups and low values of the pressure drop. It is experimentally observed that these flow regimes are often characterised by strong drop entrainment and/or high amplitude interfacial waves. The standard closure relations cannot predict the effects of these phenomena on the wall- and interfacial-shear stresses, which is the most probable reason for high prediction errors. It appears that oil and water wall-shear stresses, that satisfied the two-fluid-model equations, can be both smaller and larger than the wall-shear stress in the corresponding single-phase flow. Reduction of the wall-shear stress occurs when the corresponding phase is in the laminar or transition-to-turbulent regime. The component of the total wall-shear stress due to the single-phase-like turbulence is less dominant than the component due to the multi-phase-flow phenomena, when the phase-Reynolds number is smaller than some critical value. An increase of the phase-Reynolds number diminishes the influence of the multi-phase flow related phenomena on the wall-shear stress. This leads to a better model accuracy for the experimental points with high phase-Reynolds numbers. The flow-rates of the experimental points with a dispersed flow pattern are predicted by approximately the same accuracy as the corresponding pressure drop and water hold-up.

Even though the same mathematical model is used, the averaged and maximal calculation errors, when the two-fluid model is used, are higher when the phase flow-rates are calculated. The most probable reasons for different model accuracies, depending on the calculated variables, are different measurement uncertainties of the input variables and a high sensitivity of the calculated phase flow-rates on even a small change of the water hold-up for certain flow regimes. It was reported by Rodriguez and Oliemans (2006) that for these flow regimes, the pressure drop and water hold-up measurement uncertainties are significantly higher than the uncertainties in the flow-rate measurements.

In order to address an effect of the interfacial waves and drop entrainment on the wall- and interfacial-shear stress, parametric studies have been conducted. A parametric study of the interfacial waves shows that the mean oil and water mass-fluxes can generate very different wall-shear stresses depending on the assumed state of the oil–water interface. The wall-shear stresses calculated by the standard closure relations and with an assumption of a smooth interface, significantly differ from the wall-shear stresses that satisfy the momentum equation for the oil and water phases. If interfacial waves of certain amplitudes are considered, the difference between the experimentally determined and calculated wall-shear stresses can be considerably reduced. This parametric study predicts that only high amplitude waves have a significant effect on the wall-shear stresses.

Two different routes are adopted in a parametric study of drop entrainment. The two-dispersion model assumes that drop entrainment leads to formation of upper and lower dispersions. The mixture properties of the dispersions are calculated as in the homogeneous model. The wall-shear stress is affected by the changed fluid properties of the lower and upper layers, compared to the properties of the pure water and oil phases. The results for the experimental points with $\varepsilon_w > 0.5$, obtained by the two-dispersion model, are improved for the oil velocity. The prediction accuracy of the water velocity stays approximately the same as the one obtained by the standard two-fluid model. However, the two-dispersion model predicts too small a water velocity for four experimental points which are otherwise accurately predicted by the standard two-fluid model (with an error smaller then 30%).

For most of the experimental points, the entrainment parameters for $\varepsilon_w > 0.5$ are close to those found by Valle and Kvandal (1995). However, unphysical entrainment parameters are obtained for all experimental points with $\varepsilon_w < 0.5$. For those points, the Reynolds number of the thicker, oil-dominated layer is not particularly high, which means that turbulence is not strong enough to homogeneously dispersed the water drops. It is concluded that for these points the assumptions behind the two-dispersion model are not met.

In another approach, drop entrainment is taken into account by an extra term in the phase momentum equations. This term represents the exchange of the entrained-drop momentum with the host layer. The oil-velocity results are improved significantly for the experimental points with $\varepsilon_w > 0.5$, while the water velocity is predicted with a similar, relatively high, accuracy as by the standard two-fluid model. The errors in predicting the water and oil velocities in case of a thin layer of water could not be reduced with the two-fluid model with entrainment. These stay as high as those produced by the standard model.

The resulting entrainment flow-rates, for $\varepsilon_w > 0.5$, are in the same range as the experimentally found values by Valle and Kvandal (1995). This suggests that the assumptions behind the two-fluid model with entrainment are more realistic than those used for the derivation of the two-dispersion model. Both models suggest that drop entrainment is not the main reason for high prediction errors when the water forms a thin layer at the bottom of the pipe. However, detailed experimental data on interfacial-wave amplitudes and frequencies, as well as on entrainment rates are necessary to validate the findings of these parametric studies.

Acknowledgements

We would like to thank Shell Exploration and Production B.V. for providing financial support for this research. Dr. Roel Kusters and Prof. Neima Brauner are kindly acknowledged for their suggestions and careful reading of the paper.

References

Angeli, P., Hewitt, G., 2000. Flow structure in horizontal oil–water flow. Int. J. Multiphase Flow 26, 1117–1140.

Arirachakaran, S., Oglesby, K., Malinowsky, M., Shoham, O., Brill, J., 1989. An analysis of oil/water flow phenomena in horizontal pipes. SPE Professional Product Operating Symposium.

Brauner, N., 2001. The prediction of dispersed flows boundaries in liquid–liquid and gas–liquid systems. Int. J. Multiphase Flow 27, 885–910.

Brauner, N., Moalem Maron, D., 1991. Flow pattern transitions in two phase liquid–liquid horizontal tubes. Int. J. Multiphase Flow 18, 123–140.

Brauner, N., Moalem Maron, D., Rovinsky, J., 1998. A two-fluid model for stratified flows with curved interfaces. Int. J. Multiphase Flow 24, 975–1004.

Elseth, G., 2001. An experimental study of oil–water flow in horizontal pipes. Ph.D. thesis, The Norwegian University of Science and Technology, Porsgrunn, Norway.

Fernandino, M., Ytrehus, T., 2006. Determination of flow sub-regimes in stratified airwater channel flow using ldv spectra. Int. J. Multiphase Flow 32, 436–446.

Guet, S., Rodriguez, O.H.M., Oliemans, R.V.A., Brauner, N., 2006. An inverse dispersed multiphase flow model for liquid production rate determination. Int. J. Multiphase Flow 32, 553–567.

Haaland, S.E., 1983. Simple and explicit formulas for the friction factor in turbulent flow. J. Fluids Eng. – Trans ASME 103, 89–90.

Lodahl, C., Sumer, B., Fredsoe, J., 1998. Turbulent combined oscillatory flow and current in a pipe. J. Fluid Mech. 373, 313–348.

Lovick, J., Angeli, P., 2004. Experimental studies on the dual continuous flow pattern in oil–water flows. Int. J. Multiphase Flow 30, 139–157.

Rodriguez, O.M.H., Mudde, R.F., Oliemans, R.V.A., 2004. Inversion of multiphase flow models for multiphase well logging: larger diameters and slightly inclined pipes. 4th North American Conference on Multiphase Technology. BHR Group Limited, UK.

Rodriguez, O.M.H., Oliemans, R.V.A., 2006. Experimental study on oil/water flow in horizontal and slightly inclined pipes. Int. J. Multiphase Flow 32, 323–343.

Smolentsev, S., Miraghaie, R., 2005. Study of a free surface in open-channel water flows in the regime from weak to strong turbulence. Int. J. Multiphase Flow 31, 921–939.

Trallero, J., 1995. Oil–water flow patterns in horizontal pipes. Ph.D. Thesis, University of Tulsa, OK, USA.

Ullmann, A., Brauner, N., 2004. Closure relations for the shear stresses in two-fluid models for core-annular flow. Int. J. Multiphase Flow 16, 355–387.

Ullmann, A., Brauner, N., 2006. Closure relations for two-fluid models for two-phase stratified smooth and stratified wavy flows. Int. J. Multiphase Flow 32, 82–105.

Ullmann, A., Zamir, M., Gat, S., Brauner, N., 2003. Multi-holdups in co-current stratified flow in inclined tubes. Int. J. Multiphase Flow 29, 1565–1581.

Valle, A., Kvandal, H.-K., 1995. Pressure drop and dispersion characteristics of separated oil/water flow. In: Celata, G., Shah, R. (Eds.), Proceedings of the First International Symposium on Two-Phase Flow Modelling and Experimentation. Edizioni ETS, Pisa, Italy.